

The Vertical Coupling Method: A two layer approach for Coupling 1D/2D Shallow Water Flow Models

Chinedu Nwaigwe ^{*1} and Andreas S. Dedner ^{†1}

¹Centre for Scientific Computing and Warwick Mathematics Institute, University of Warwick, United Kingdom

Received: never; **final revision:** never; **published:** never.

Abstract

In this paper, we propose a novel approach for coupling 2D/1D shallow water flow models. Efficiently coupling these models is vital for simulating the flow and flooding of open channels. Currently, existing methods couple the models either at the channel lateral boundaries (lateral methods) or at the location, along the channel flow direction, where the two sub-domains intersect (frontal methods). We classify these methods as horizontal methods since the coupling points are on the horizontal plane. The limitations of these methods include their inability to recover the 2D channel flow structure during flooding without losing efficiency, and their inability to switch between lateral and frontal methods, based on the problem. Here, we propose a new paradigm which is to think of the channel flow as a two layer flow. This leads to the vertical coupling method (VCM) which is able to recover 2D channel flow structure without losing efficiency, switch types depending on the flow and is a superset of some existing methods. The VCM is based on a user chosen elevation above which the user considers the channel to be full. From this elevation, all other flow quantities are defined including the two layers. The flows in the lower and upper layers are assumed to be 1D and 2D respectively, and the appropriate flow models with exchange terms are derived. The 2D shallow water flow model is retained for the floodplains. Finite volume methods (FVM) are formulated for the flood model; the FVM with the operator splitting approach are also formulated to solve and couple the two layer channel flow models. We show that the resulting method (i) is well-balanced (ii) preserves the "no-numerical" flooding property (iii) preserves conservation properties and (iv) adapts to the flow situation.

1 Introduction

It is known that 1D Saint Venant Model can be used to simulate open channel flows but it becomes inadequate if the channel overflows. However, multi-dimensional (even 2D) simulations are quite computationally expensive. This has led to coupling 1D channel simulation with 2D floodplain simulations which has become the subject of much research amongst applied Mathematicians, scientists and engineers.

River/floodplain coupling simulations started as quasi 2D models in which floodplains are represented by storage cells, then coupled with an existing 1D river model [9, 4]. These approaches could not allow to simulate the fluid dynamics in the floodplains [10]. Therefore, the search for methods that allow to simultaneously simulate the flow in both the river and the floodplains continues.

*nwaigwe@warwick.ac.uk

†a.s.dedner@warwick.ac.uk

In [5], the coupling of 1D/2D models was achieved, numerically, by including the 2D numerical fluxes into the finite volume scheme for the 1D model. [8] utilized the theory of characteristics to couple 1D/2D models through some matching conditions defined at the 2D/1D interface points. In [22], the 1D river model and the 2D non-inertia model were also coupled where the water level differences between the flows in the two domains are used to calculate the interacting discharges in the sub-domains.

Methods based on post-processing the separately computed solutions are presented in [17], see also [16]. At 2D/1D interface, each model computes its own solution from which the total water volume in a 1D cell and all its adjacent 2D cells is computed. Then, the water height for 2D cells and the wetted Area for the associated 1D cell are found. In [19], the methods have been applied to Tiber River, Rome.

In [15], the 1D model including the coupling terms were classically derived from the full 3D inviscid Euler's equations and an optimal control process applied to couple the models. These models have been numerically treated with the finite volume method [10] where the discrete exchange term, which lead to globally well-balanced scheme, is proposed. This approach superposes a 2D grid over the 1D channel grid and convergence is achieved using a Schwartz-like iterative algorithm.

A known difficulty for coupling 2D/1D shallow water models is the computation of the channel flow lateral discharge because the 1D channel flow model does not have an equation for it. In [11], this channel lateral discharge was set to zero, while [12] adopted an iterative technique that uses the solution of successive Riemann problems to estimate the transverse velocity. This difficulty in computing the channel lateral discharge remains challenging.

As pointed out in [21], another issue is the 1D assumption on the channel flow during flooding, which is inadequate. It was proposed to compute different discharges for each channel lateral boundary. However, the free-surface and x -velocity component were still assumed to be laterally constant across the channel, while the 2D Shallow water equation was used as an ad-hoc model to compute the lateral discharge. This improved the results but still does not recover the complete 2D flow structure during flooding. Consequently, efficient methods that recover the 2D flow structure during flooding are still lacking. Although frontal coupling methods recover 2D flow structure but they loose efficiency because they compute the 2D solutions at all times.

Moreover, most of the existing methods need to know, a priori, the location of flooding but in reality, flooding locations vary with time, so we desire methods that can automatically detect them (the flooding regions). Currently, methods that automatically resolves both lateral and frontal coupling problems, or that are superset of existing methods, are rare or even non-existent.

Consequently, the goal of this paper is to propose a method, the vertical coupling method (VCM), that (i) recovers the 2D flow structure during flooding while reverting back to 1D simulation if there is no flooding. (ii) automatically detects flooding regions. (iii) is able to automatically resolve both lateral and frontal flooding problem and (iv) is a superset of some existing methods.

The VCM is based on partitioning an overflowing channel flow into two vertical layers where the flows in the lower and upper layers are considered as 1D and 2D respectively. This then enables us to derive two coupled models (one for each layer) which together represent the channel flow model. The rest of the paper are organised as follows. The model equations are derived in section 2. Here, we start by presenting the background details of the VCM in section 2.1, then derive the lower and upper layer flow models in sections 2.2 and 2.3 respectively, then the complete two layer channel flow models are summarised in section 2.4. The floodplain flow model is presented in section 2.5. The numerical schemes for the flood flow model is presented in section 3. Then a detailed numerical algorithm flow for the coupled channel flow models is presented in section 4 and the properties of the method are considered in section 5 where we prove that the method is well-balanced, preserves no-numerical flooding and mass conservative. The numerical approximation of the solutions of the coupled channel models without exchange

terms are presented in section 4.5. Numerical experiments are presented in section 6 to access the performance of the method while the paper is concluded in section 7.

2 Mathematical Models for the Fluid Dynamics

This section presents the model equations for the flood flow and derive, in detail, the two layer models for the channel flow.

2.1 Background

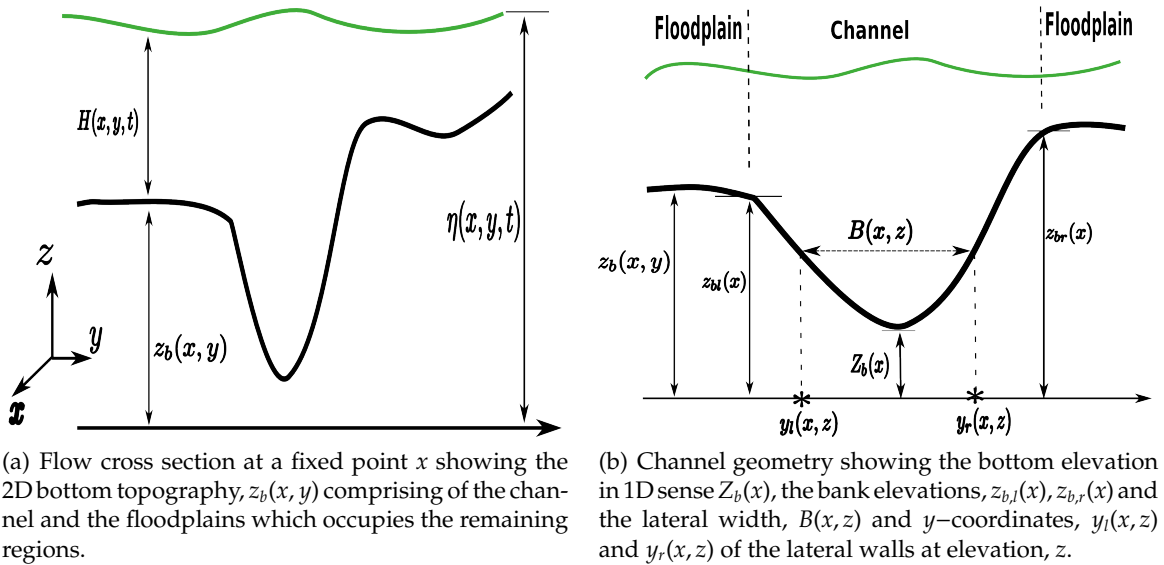


Figure 1: Illustration of flow cross section (left) and channel geometry (right).

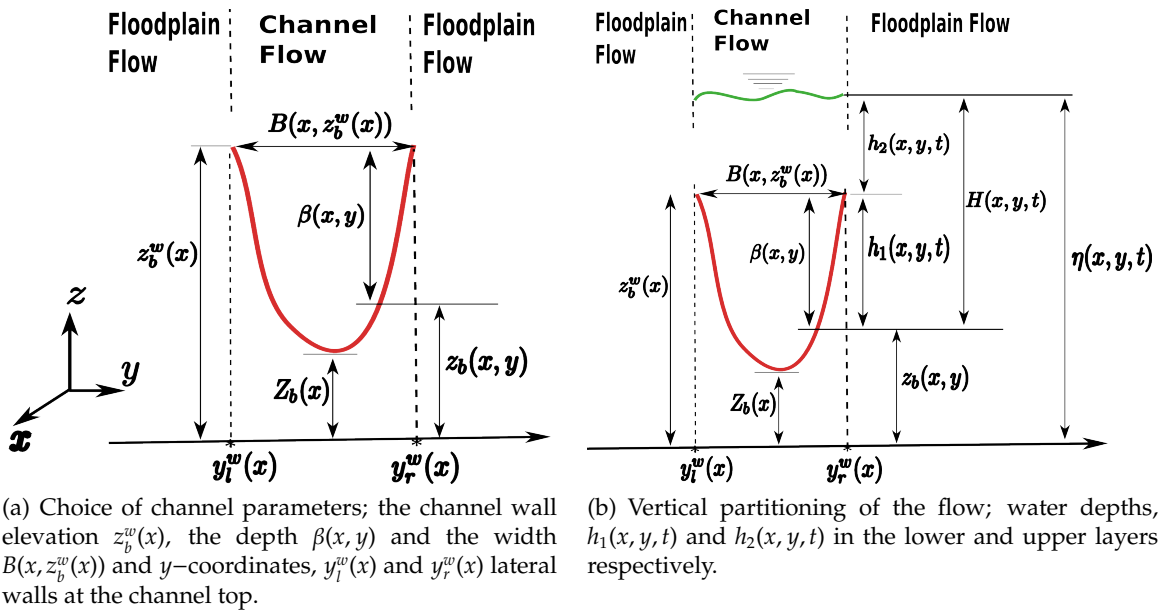


Figure 2: VCM channel definitions (left) and flow partitioning (right)

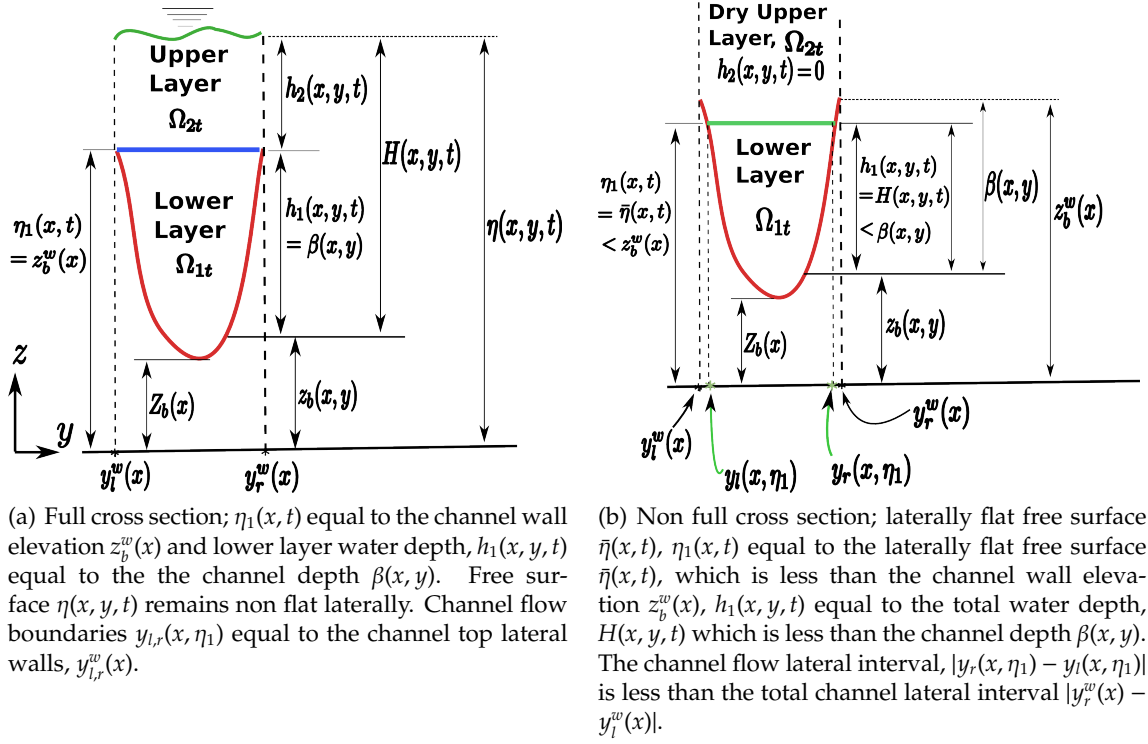


Figure 3: The two layers in the VCM in the case of full channel (left) and the non full case (right)

Consider the flow of water over the fixed horizontal 2D domain, $\Omega_H \subset \mathbb{R}^2$ such that the flow at time, t occupies the 3D domain, Ω_t defined by

$$\Omega_t = \{(\vec{X}, z) \in \mathbb{R}^3 : \vec{X} = (x, y) \in \Omega_H, z_b(\vec{X}) \leq z \leq \eta(\vec{X}, t)\}, \quad (1)$$

bounded below by a fixed bottom, $z = z_b(\vec{X})$ and above by the water free-surface elevation, $\eta(\vec{X}, t)$ given by

$$\eta(\vec{X}, t) = z_b(\vec{X}) + H(\vec{X}, t), \quad (2)$$

and $H(\vec{X}, t)$ is the depth of fluid at time, t , see figure 1(a) which depicts a cross section of the 3D flow domain. The bottom topography, $z_b(\vec{X})$ consists of a channel and floodplains.

2.1.1 Channel Geometry: Figure 1(b) shows the flow cross section indicating the channel geometry. The channel whose length lies along the x -axis (frontal direction) and the width, along the y -axis (lateral direction) has left and right bank elevations, $z_{b,l}(x)$ and $z_{b,r}(x)$ respectively. Given an elevation, z above the reference $z = 0$, then the function, $B(x, z)$ gives the channel lateral width, while $y_l(x, z)$ and $y_r(x, z)$ are the y -coordinates of the left and right lateral wall boundaries respectively at the elevation, z . So that

$$B(x, z) = y_r(x, z) - y_l(x, z) \quad \forall z \in \mathbb{R}. \quad (3)$$

We also define $Z_b(x)$ to be the channel bottom topography in 1D sense; we take it to be

$$Z_b(x) = \min_y z_b(x, y). \quad (4)$$

Note that the width functions, $B(x, z)$, $y_l(x, z)$, $y_r(x, z)$ satisfy the following:

$$B(x, z) = 0, \quad y_r(x, z) = y_l(x, z) \quad \text{for all } z < Z_b(x), \quad (5)$$

see figure 1(b). We also assume the the channel height function is known, that is given the cross section area, $A(x, t)$ we define the channel height function, $\mathcal{H}(A, z_b)$ as the water depth measured from the bottom elevation, $z_b(\vec{X})$ to the free surface.

2.1.2 The VCM Background Given the channel geometry above, the formulation of the VCM starts by choosing an elevation, $z_b^w(x) \geq Z_b(x)$ above which the channel is considered full, see figure 2(a). This elevation is completely decided by the user; the only constraint is that it must not be less than $Z_b(x)$ as defined in (4). So, $z_b^w(x)$ becomes the channel top and is referred to as the maximum wall elevation defined as follows:

Definition 2.1 (Maximum channel wall elevation, $z_b^w(x)$) *The maximum channel wall elevation at cross section x , is the minimum elevation of the channel banks above which flooding is said to have occurred [20, 21].*

Once $z_b^w(x)$ has been decided, other quantities are derived, see figure 2(a). The lateral width and the y -coordinates of the lateral wall boundaries at the top ($z = z_b^w(x)$) becomes $B(x, z_b^w(x))$ and $y_{l,r}^w(x) := y_{l,r}(x, z_b^w(x))$ respectively. Therefore, we consider the channel flow only within the region $y_l^w(x) < y < y_r^w(x)$, and the flood flow in the rest regions, $-\infty < y < y_l^w(x)$ and $y_r^w(x) < y < \infty$, see figure 2(a). As noted above, the floodplain flows will be simulated with the 2D shallow water models (see section 2.5), therefore we focus on formulating the models for the flow in the channel region.

Notice from figure 2(a) that the closer the chosen $z_b^w(x)$ is to $Z_b(x)$, the smaller the channel flow region, $y_l^w(x) < y < y_r^w(x)$, hence the larger the floodplain flow region. In particular, choosing $z_b^w(x)$ equal to $Z_b(x)$ means to consider floodplain flow everywhere, that is a full 2D simulation. So, different choices $z_b^w(x)$ lead to different approaches.

Having identified the channel and floodplain flow regions, we now concentrate on the channel region. First, we note that the following condition holds:

$$z_b(\vec{X})|_{y=y_l(x,z), y_r(x,z)} = z \quad \forall z \in [Z_b(x), z_b^w(x)]. \quad (6)$$

We also extend the definition of the width functions, $B(x, z)$, $y_{l,r}(x, z)$ to the region above the top (that is where $z \geq z_b^w(x)$) as follows:

$$B(x, z) = B(x, z_b^w(x)) \quad \text{and} \quad y_{l,r}(x, z) = y_{l,r}^w(x) \quad \forall z \geq z_b^w(x), \quad (7)$$

see figure 2(a). We now proceed to define the other important quantities for the channel flow.

Definition 2.2 (Channel Depth) *The channel depth, $\beta(\vec{X})$ is the laterally varying height between the channel bed and the chosen elevation, $z_b^w(x)$, that is*

$$\beta(\vec{X}) = z_b^w(x) - z_b(\vec{X}), \quad y_l^w(x) \leq y \leq y_r^w(x), \quad (8)$$

see figure 2(a).

We also introduce the critical area defined as follows.

Definition 2.3 (Critical Area) *The critical area, $A_c(x)$ is the wetted cross sectional area of an exactly filled cross section. That is, the wetted cross sectional area when the water level is exactly at the chosen elevation, $z_b^w(x)$. It is defined as*

$$A_c(x) = \int_{y_l(x, z_b^w(x))}^{y_r(x, z_b^w(x))} \beta(\vec{X}) dy. \quad (9)$$

We assume that the channel is never completely dry, namely $\exists y \in (y_l^{wv}(x), y_r^{wv}(x))$ such that $\eta(\vec{X}, t) > z_b(\vec{X})$ for all t . Note that if the water level is below the $z_b^{wv}(x)$, then the y -coordinates of the flow (wetted) lateral walls are different from $y_{l,r}^{wv}(x)$, so we give a general definition of these coordinates.

Definition 2.4 (Channel Flow Lateral Boundaries) Let $y_l^*(x, t)$ and $y_r^*(x, t)$ denote the y -coordinates of the left and right channel flow lateral boundaries, then

$$\begin{aligned} y_l^*(x, t) &:= \min\{y : \eta(\vec{X}, t) > z_b(\vec{X}), y \geq y_l(x, z_b^{wv}(x))\}, \\ y_r^*(x, t) &:= \max\{y : \eta(\vec{X}, t) > z_b(\vec{X}), y \leq y_r(x, z_b^{wv}(x))\}. \end{aligned} \quad (10)$$

Note that if there is water everywhere in the channel, then $y_{l,r}^*(x, t) = y_{l,r}^{wv}(x)$.

Remark 2.1 (Channel Assumption) We assume that the channel never goes dry anywhere between the lateral wall boundaries, namely

$$\eta(\vec{X}, t) > z_b(\vec{X}) \quad \forall y \in (y_l^*(x, t), y_r^*(x, t)).$$

Definition 2.5 (Average Free Surface) With the flow lateral boundaries known, we can define the laterally averaged free surface elevation, namely

$$\bar{\eta}(x, t) = \frac{1}{y_r^*(x, t) - y_l^*(x, t)} \int_{y_l^*(x, t)}^{y_r^*(x, t)} \eta(\vec{X}, t) dy. \quad (11)$$

Next, we now say exactly what we mean by a full channel.

Definition 2.6 (Full Channel) We say the cross section is full if

$$H(\vec{X}, t) \geq \beta(\vec{X}) \quad \forall y \in (y_l^{wv}(x), y_r^{wv}(x)). \quad (12)$$

This means that if the channel is full, then the following hold:

•

$$A(x, t) := \int_{y_l^{wv}(x)}^{y_r^{wv}(x)} H(\vec{X}, t) dy \geq \int_{y_l^{wv}(x)}^{y_r^{wv}(x)} \beta(\vec{X}) dy = A_c(x), \quad (13)$$

where $A(x, t)$ is the total water in the cross section.

•

$$\bar{\eta}(x, t) \geq z_b^{wv}(x) \quad (14)$$

Because

$$\begin{aligned} \bar{\eta}(x, t) &:= \frac{1}{y_r^*(x, t) - y_l^*(x, t)} \int_{y_l^*(x, t)}^{y_r^*(x, t)} \eta(\vec{X}, t) dy = \frac{1}{y_r^*(x, t) - y_l^*(x, t)} \int_{y_l^*(x, t)}^{y_r^*(x, t)} (H(\vec{X}, t) + z_b(\vec{X})) dy \\ &\geq \frac{1}{y_r^*(x, t) - y_l^*(x, t)} \int_{y_l^*(x, t)}^{y_r^*(x, t)} (\beta(\vec{X}) + z_b(\vec{X})) dy \\ &= \frac{1}{y_r^*(x, t) - y_l^*(x, t)} \int_{y_l^*(x, t)}^{y_r^*(x, t)} z_b^{wv}(x) dy = z_b^{wv}(x). \end{aligned}$$

Since we want to retain 1D flow assumptions if the channel is not full, then we make the following assumption to allow consistency with 1D formulations.

Definition 2.7 (1D Consistency Assumption) *If the channel is not full, then the lateral variation in free surface elevation, $\eta(\vec{X}, t)$ is negligible and the free surface can be taken to be its lateral average, $\bar{\eta}(x, t)$. This simply means that we assume the free surface to be laterally flat. This is exactly the 1D assumption and allows to apply 1D modelling whenever the channel is not full.*

Next, we define the following elevation:

Definition 2.8 (Time Dependent Interface) *The time dependent interface, $\eta_1(x, t)$ is the elevation defined as,*

$$\eta_1(x, t) = \min(\bar{\eta}(x, t), z_b^w(x)). \quad (15)$$

Proposition 2.1 $y_{l,r}^*(x, t) = y_{l,r}(x, \eta_1)$.

Proof: Case 1 : If the channel is full (see figure 3(a)), then
(i) by definition 2.6,

$$\bar{\eta}(x, t) \geq z_b^w(x). \text{ Hence } \eta_1 := \min(\bar{\eta}(x, t), z_b^w(x)) = z_b^w(x).$$

(ii) By definition 2.4, the lateral walls are

$$y_{l,r}^*(x, t) := y_{l,r}(x, z_b^w(x)) = y_{l,r}(x, \eta_1).$$

Case 2 : If the channel is not full (see figure 3(b)), then

$$\bar{\eta}(x, t) \leq z_b^w(x), \text{ so } \eta_1 := \min(\bar{\eta}(x, t), z_b^w(x)) = \bar{\eta}(x, t).$$

And definition 2.7 requires free surface to be constant and equal to the average, $\bar{\eta}(x, t)$, hence the free surface at the lateral walls is $\bar{\eta}(x, t)$. So, the lateral boundaries are $y_{l,r}^*(x, t) = y_{l,r}(x, \bar{\eta}) = y_{l,r}(x, \eta_1(x, t))$. \square

Hence, the flow lateral walls, $y_{l,r}^*(x, t)$ are replaced with $y_{l,r}(x, \eta_1)$. We can now identify the channel flow domain, Ω_{ct} at time, t as:

$$\Omega_{ct} = \{(\vec{X}, z) \in \mathbb{R}^3 : y_l(x, \eta_1(x, t)) \leq y \leq y_r(x, \eta_1(x, t)), z_b(\vec{X}) \leq z \leq \eta(\vec{X}, t)\}. \quad (16)$$

We now partition the channel flow into two vertical layers.

Definition 2.9 (Flow Partitions) *The channel flow is decomposed into two layers by defining the following quantities:*

$$H(\vec{X}, t) = \eta(\vec{X}, t) - z_b(\vec{X}), \quad y_l(x, \eta_1(x, t)) \leq y \leq y_r(x, \eta_1(x, t)), \quad (17)$$

$$h_1(\vec{X}, t) = \min(H(\vec{X}, t), \beta(\vec{X})), \quad y_l(x, \eta_1(x, t)) \leq y \leq y_r(x, \eta_1(x, t)), \quad (18)$$

$$h_2(\vec{X}, t) = H(\vec{X}, t) - h_1(\vec{X}, t), \quad y_l(x, \eta_1(x, t)) \leq y \leq y_r(x, \eta_1(x, t)), \quad (19)$$

where $h_1(\vec{X}, t)$ and $h_2(\vec{X}, t)$ are the water depth in the lower and upper layers respectively, see figure 2(b). Hence, the sum, $h_1(\vec{X}, t) + z_b(\vec{X})$ defines the top of the lower layer. By our 1D consistency assumptions above, this sum, $h_1(\vec{X}, t) + z_b(\vec{X})$ is required to be independent of y . This is so because in the case when $h_2(\vec{X}, t)$ is all zero in the cross-section, this sum is the free-surface and less than or equal to $z_b^w(x)$, so must be laterally flat (independent of y). The proof of this is to show that

$$h_1(\vec{X}, t) + z_b(\vec{X}) = \eta_1(x, t). \quad (20)$$

see [20].

Hence, $\eta_1(x, t)$ as given (15) is the time varying interface position between the two layers. We now partition the channel flow domain into the following two sub-domains which we call layers :

$$\Omega_{1t} = \{(\vec{X}, z) \in \mathbb{R}^3 : y_l(x, \eta_1(x, t)) \leq y \leq y_r(x, \eta_1(x, t)), z_b(\vec{X}) \leq z \leq \eta_1(x, t)\}, \quad (21)$$

$$\Omega_{2t} = \{(\vec{X}, t) \in \mathbb{R}^3 : y_l(x, \eta_1(x, t)) \leq y \leq y_r(x, \eta_1(x, t)), \eta_1(x, t) \leq z \leq \eta(\vec{X}, t)\}. \quad (22)$$

In summary, the lower layer begins at the bottom of the channel and ends at $\eta_1(x, t)$, while the upper layer is from $\eta_1(x, t)$ to the free-surface level, $\eta(\vec{X}, t)$. In the next sections we formulate the equations of fluid motion in each layer, based on the assumptions, we have stated so far.

2.1.3 Fundamental Equations: Under the assumption of hydrostatic pressure, the flow in the domain, Ω_{ct} is governed by the following Free-Surface Euler Equations:

$$\partial_x u(\vec{X}, z, t) + \partial_y v(\vec{X}, z, t) + \partial_z w(\vec{X}, z, t) = 0, \quad (23)$$

$$\begin{aligned} \partial_t u(\vec{X}, z, t) + \partial_x (u^2(\vec{X}, z, t)) + \partial_y (u(\vec{X}, z, t)v(\vec{X}, z, t)) \\ + \partial_z (u(\vec{X}, z, t)w(\vec{X}, z, t)) = -g\partial_x \eta(\vec{X}, t), \end{aligned} \quad (24)$$

$$\begin{aligned} \partial_t v(\vec{X}, z, t) + \partial_x (u(\vec{X}, z, t)v(\vec{X}, z, t)) + \partial_y (v^2(\vec{X}, z, t)) \\ + \partial_z (v(\vec{X}, z, t)w(\vec{X}, z, t)) = -g\partial_y \eta(\vec{X}, t), \end{aligned} \quad (25)$$

in Ω_{ct} and the following boundary conditions:

$$\left(u(\vec{X}, z, t)\partial_x z_b(\vec{X}) + v(\vec{X}, z, t)\partial_y z_b(\vec{X}) - w(\vec{X}, z, t) \right) \Big|_{z=z_b(\vec{X})} = 0, \quad (26)$$

$$\left(\partial_t \eta(\vec{X}, t) + u(\vec{X}, z, t)\partial_x \eta(\vec{X}, t) + v(\vec{X}, z, t)\partial_y \eta(\vec{X}, t) - w(\vec{X}, z, t) \right) \Big|_{z=\eta(\vec{X}, t)} = 0, \quad (27)$$

where $\rho, (u, v, w)^T$ and P are the fluid density, velocity vector and pressure at point (\vec{X}, z) at time, t and P_{atm} is the atmospheric pressure, here taken to be zero.

2.2 The Lower Layer Flow Model

The lower layer flow is assumed to be 1D; this allows us to assume further that the lateral variations in free-surface elevation do not have any impact on the lower layer flow. Therefore, using the averaged free-surface, $\bar{\eta}(x, t)$, instead of $\eta(\vec{X}, t)$, the Free-Surface Euler Equations above reduce to the following:

$$\partial_x u(\vec{X}, z, t) + \partial_y v(\vec{X}, z, t) + \partial_z w(\vec{X}, z, t) = 0, \quad (28)$$

$$\partial_t u(\vec{X}, z, t) + \partial_x (u^2(\vec{X}, z, t)) + \partial_y (u(\vec{X}, z, t)v(\vec{X}, z, t)) + \partial_z (u(\vec{X}, z, t)w(\vec{X}, z, t)) = -g\partial_x \bar{\eta}(x, t), \quad (29)$$

in Ω_{1t} .

$$\left(u(\vec{X}, z, t)\partial_x z_b(\vec{X}) + v(\vec{X}, z, t)\partial_y z_b(\vec{X}) - w(\vec{X}, z, t) \right) \Big|_{z=z_b(\vec{X})} = 0, \quad (30)$$

$$\left(\partial_t \bar{\eta}(x, t) + u(\vec{X}, z, t)\partial_x \bar{\eta}(x, t) - w(\vec{X}, z, t) \right) \Big|_{z=\bar{\eta}(x, t)} = 0. \quad (31)$$

2.2.1 Mass Conservation Equation for Lower Layer: We define the area of wetted cross section, $A_1(x, t)$, the section averaged volumetric discharge, $Q_1(x, t)$ and section averaged velocity, $\underline{u}_1(x, t)$, for the lower layer, as follows:

$$Q_1(x, t) = \int_{y_l(x, \eta_1(x, t))}^{y_r(x, \eta_1(x, t))} \int_{z_b(\vec{X})}^{\eta_1(x, t)} u(\vec{X}, z, t) dz dy, \quad (32)$$

$$A_1(x, t) = \int_{y_l(x, \eta_1(x, t))}^{y_r(x, \eta_1(x, t))} \int_{z_b(\vec{X})}^{\eta_1(x, t)} dz dy = \int_{y_l(x, \eta_1(x, t))}^{y_r(x, \eta_1(x, t))} h_1(\vec{X}, t) dy, \quad (33)$$

$$\underline{u}_1(x, t) = \frac{Q_1(x, t)}{A_1(x, t)} = \frac{1}{A_1(x, t)} \int_{y_l(x, \eta_1(x, t))}^{y_r(x, \eta_1(x, t))} \int_{z_b(\vec{X})}^{\eta_1(x, t)} u(\vec{X}, z, t) dz dy. \quad (34)$$

Before we proceed, let us recall the following important assertions.

Lemma 2.1 Let A_c and A be defined in (9) and (13) respectively, and

$$A_c^*(x, t) = \int_{y_l(x, \eta_1(x, t))}^{y_r(x, \eta_1(x, t))} \beta(\vec{X}) dy, \quad (35)$$

then

$$\min(A(x, t), A_c^*(x, t)) = \min(A(x, t), A_c(x)). \quad (36)$$

Proof: See [20] for the proof. \square

A result very useful to numerical implementation of the VCM follows.

Theorem 2.1 Let A_c , A , A_1 and A_c^* be defined in (9), (13), (33) and (35) respectively, then

$$A_1(x, t) = \min(A(x, t), A_c(x)). \quad (37)$$

Proof: See [20] for the proof. \square

We now proceed to derive the model equations for the lower layer. Integrating the equation (28) over the lower layer cross section, we have

$$\int_{y_l(x, \eta_1(x, t))}^{y_r(x, \eta_1(x, t))} \int_{z_b(\vec{X})}^{\eta_1(x, t)} (\partial_x u(\vec{X}, z, t) + \partial_y v(\vec{X}, z, t) + \partial_z w(\vec{X}, z, t)) dz dy = 0. \quad (38)$$

Evaluating the above integral by applying the Leibniz rule and using the kinematic boundary condition (30), we have

$$\partial_t A_1(x, t) + \partial_x Q_1(x, t) = - \int_{y_l(x, \eta_1(x, t))}^{y_r(x, \eta_1(x, t))} S(\vec{X}, t) dy, \quad (39)$$

where

$$S(\vec{X}, t) = \left[w(\vec{X}, z, t) - u(\vec{X}, z, t) \partial_x \eta_1(x, t) - \partial_t \eta_1(x, t) \right] \Big|_{z=\eta_1(x, t)}, \quad (40)$$

and $\int_{y_l(x, \eta_1(x, t))}^{y_r(x, \eta_1(x, t))} S(\vec{X}, t) dy$ is a mass exchange term between the two layers.

2.2.2 Momentum Equation for Lower Layer: To derive the momentum equation for the lower layer, we integrate equation (29) over the lower layer cross section, namely

$$\begin{aligned}
& \int_{y_l(x, \eta_1(x, t))}^{y_r(x, \eta_1(x, t))} \int_{z_b(\vec{X})}^{\eta_1(x, t)} \partial_t u(\vec{X}, z, t) dz dy + \int_{y_l(x, \eta_1(x, t))}^{y_r(x, \eta_1(x, t))} \int_{z_b(\vec{X})}^{\eta_1(x, t)} \partial_x (u^2(\vec{X}, z, t)) dz dy \\
& + \int_{y_l(x, \eta_1(x, t))}^{y_r(x, \eta_1(x, t))} \int_{z_b(\vec{X})}^{\eta_1(x, t)} \partial_y (u(\vec{X}, z, t) v(\vec{X}, z, t)) dz dy + \int_{y_l(x, \eta_1(x, t))}^{y_r(x, \eta_1(x, t))} \int_{z_b(\vec{X})}^{\eta_1(x, t)} \partial_z (u(\vec{X}, z, t) w(\vec{X}, z, t)) dz dy \\
& = - \int_{y_l(x, \eta_1(x, t))}^{y_r(x, \eta_1(x, t))} \int_{z_b(\vec{X})}^{\eta_1(x, t)} g \partial_x \bar{\eta}(x, t) dz dy = -g \partial_x \bar{\eta}(x, t) \int_{y_l(x, \eta_1(x, t))}^{y_r(x, \eta_1(x, t))} \int_{z_b(\vec{X})}^{\eta_1(x, t)} dz dy \\
& = -g A_1(x, t) \partial_x \bar{\eta}(x, t). \quad (41)
\end{aligned}$$

The above equation gives

$$\partial_t Q_1(x, t) + \partial_x \left(\frac{Q_1^2(x, t)}{A_1(x, t)} \right) = -g A_1(x, t) \partial_x \bar{\eta}(x, t) - \int_{y_l(x, \eta_1(x, t))}^{y_r(x, \eta_1(x, t))} (u(\vec{X}, z, t)|_{z=\eta_1(x, t)} S(\vec{X}, t)) dy, \quad (42)$$

where the last integral on the right is the momentum exchange term between the two layers.

2.3 Upper Layer Flow Model

The upper layer flow is allowed to remain fully two-dimensional, so the Free-Surface Euler Equations, (23) - (25) and (27) are applicable. However, the kinematic boundary condition on the bottom does not apply here because the bottom of the upper layer is $\eta_1(x, t)$ which is not a physical boundary that fluid particles cannot cross. Define the following quantities:

$$q_{2x}(\vec{X}, t) = \int_{\eta_1(x, t)}^{\eta(\vec{X}, t)} u(\vec{X}, z, t) dz, \quad q_{2y}(\vec{X}, t) = \int_{\eta_1(x, t)}^{\eta(\vec{X}, t)} v(\vec{X}, z, t) dz. \quad (43)$$

So that the velocities are

$$u_2(\vec{X}, t) = \frac{q_{2x}(\vec{X}, t)}{h_2(\vec{X}, t)} \quad \text{and} \quad v_2(\vec{X}, t) = \frac{q_{2y}(\vec{X}, t)}{h_2(\vec{X}, t)}, \quad (44)$$

where $\vec{q}_2(\vec{X}, t) = (q_{2x}(\vec{X}, t), q_{2y}(\vec{X}, t))^T$ is the upper layer 2D discharge vector and $\vec{u}_2(\vec{X}, t) = (u_2(\vec{X}, t), v_2(\vec{X}, t))^T$, the velocity vector for upper layer. In what follows, we derive the equations for the 2D quantities. Integrating equation (23) vertically over the upper layer, we have

$$\int_{\eta_1(x, t)}^{\eta(\vec{X}, t)} (\partial_x u(\vec{X}, z, t) + \partial_y v(\vec{X}, z, t) + \partial_z w(\vec{X}, z, t)) dz = 0. \quad (45)$$

Evaluating the integrals, the above equation gives

$$\partial_t h_2(\vec{X}, t) + \partial_x q_{2x}(\vec{X}, t) + \partial_y q_{2y}(\vec{X}, t) = S(\vec{X}, t). \quad (46)$$

Also, integrating equation (24) vertically over $\eta_1(x, t) \leq z \leq \eta(\vec{X}, t)$, applying the kinematic boundary condition on (equation (27)) and simplifying, we have

$$\begin{aligned}
& \partial_t q_{2x}(\vec{X}, t) + \partial_x \left(\frac{q_{2x}^2(\vec{X}, t)}{h_2(\vec{X}, t)} + g \frac{1}{2} h_2^2(\vec{X}, t) \right) + \partial_y \left(\frac{q_{2x}(\vec{X}, t) q_{2y}(\vec{X}, t)}{h_2(\vec{X}, t)} \right) \\
& = -g h_2(\vec{X}, t) \partial_x z_b(\vec{X}) - g h_2(\vec{X}, t) \partial_x h_1(\vec{X}, t) + u(\vec{X}, z, t)|_{z=\eta_1(x, t)} S(\vec{X}, t). \quad (47)
\end{aligned}$$

Similarly, integrating equation (25) vertically over $\eta_1(x, t) \leq z \leq \eta(\vec{X}, t)$, applying the kinematic boundary condition on (equation (27)) and simplifying, we have

$$\begin{aligned} \partial_t q_{2y}(\vec{X}, t) + \partial_x \left(\frac{q_{2x}(\vec{X}, t) q_{2y}(\vec{X}, t)}{h_2(\vec{X}, t)} \right) + \partial_y \left(\frac{q_{2y}^2(\vec{X}, t)}{h_2(\vec{X}, t)} + g \frac{1}{2} h_2^2(\vec{X}, t) \right) \\ = -g h_2(\vec{X}, t) \partial_y z_b(\vec{X}) + v(\vec{X}, z, t)|_{z=\eta_1(x,t)} S(\vec{X}, t). \end{aligned} \quad (48)$$

$S(\vec{X}, t)$ is as defined in equation (40).

2.4 Summary of Coupled Channel Flow Models

We can then summarise the channel model as the lower layer model,

$$\begin{aligned} \partial_t A_1 + \partial_x Q_1 &= - \int_{y_l(x, \eta_1(x,t))}^{y_r(x, \eta_1(x,t))} S dy, \\ \partial_t Q_1 + \partial_x Q_1^2 / A_1 &= -g A_1 \partial_x \bar{\eta} - \int_{y_l(x, \eta_1(x,t))}^{y_r(x, \eta_1(x,t))} u_{\eta_1} S dy, \end{aligned} \quad (49)$$

and the upper layer model,

$$\begin{aligned} \partial_t h_2 + \nabla \cdot \vec{q}_2 &= S, \\ \partial_t \vec{q}_2 + \nabla \cdot F^q(h_2, \vec{q}_2) &= -g h_2 \nabla(z_b + h_1) + \vec{u}_{\eta_1} S, \end{aligned} \quad (50)$$

where

$$F^q(h_2, \vec{q}_2) = (F^x, F^y), F^x = \left(\frac{q_{2x}^2}{h_2} + \frac{g}{2} h_2^2, \frac{q_{2x} q_{2y}}{h_2} \right)^T, F^y = \left(\frac{q_{2x} q_{2y}}{h_2}, \frac{q_{2y}^2}{h_2} + \frac{g}{2} h_2^2 \right)^T, \vec{u}_{\eta_1} = (u(\vec{X}, t), v(\vec{X}, t))^T \Big|_{z=\eta_1}$$

$u_{\eta_1} = u(\vec{X}, t) \Big|_{z=\eta_1}$. We make the following remarks about models derived for these two layers.

Remark 2.2 We note that the models (50) and (49) are not closed since the exchange terms and interface velocities are not known. By following the idea adopted in [3], we determine these quantities using the results of the numerical solutions of the systems without them. This procedure is outlined in the numerical algorithm in section 4.

Remark 2.3 The fact that the flow variables, such as $\eta_1(x, t)$ and $h_1(x, y, t)$ are defined using the minimum function means that the PDEs so derived may not make sense in the classical sense. However, our goal is not to study the mathematical properties of the PDEs for which rigorous definitions are required, but to use them to derive our desired numerical schemes. Therefore, we do not concern ourselves with the rigorous definitions, hence the above derivation has to be understood as a formal derivation of the governing equations under the assumption that all functions are sufficiently smooth.

2.5 Floodplain Flow Model

We describe the flow in the floodplains using the 2D Shallow water equations, namely

$$\partial_t \Pi + \nabla \cdot F(\Pi) = S(\Pi, z_b) + S_b(\Pi), \quad (51)$$

where

$$\begin{aligned} \Pi &= \begin{pmatrix} H \\ q_x \\ q_y \end{pmatrix}, \quad F(\Pi) = (F_1(\Pi), F_2(\Pi)), \\ F_1(\Pi) &= \begin{pmatrix} q_x \\ \frac{q_x^2}{H} + \frac{1}{2}gH^2 \\ \frac{q_x q_y}{H} \end{pmatrix}, \quad F_2(\Pi) = \begin{pmatrix} q_y \\ \frac{q_x q_y}{H} \\ \frac{q_y^2}{H} + \frac{1}{2}gH^2 \end{pmatrix}, \\ S_b(\Pi) &= \begin{pmatrix} 0 \\ -g\frac{n^2}{H^{7/3}}\vec{q}|\vec{q}| \end{pmatrix}, \quad S(\Pi, z_b) = \begin{pmatrix} 0 \\ -gH\partial_x z_b(\vec{X}) \\ -gH\partial_y z_b(\vec{X}) \end{pmatrix}, \end{aligned} \quad (52)$$

where n is manning coefficient, S_b is the friction term and $S(\Pi, z_b)$ is the source term due to bottom topography term.

3 Numerical Schemes for uncoupled Flood and Channel Flow Models

In this section, we present the numerical schemes for the flood model, (51) and for a conventional channel model without any coupling nor exchange terms.

3.1 Scheme for 2D Flood Flow Model

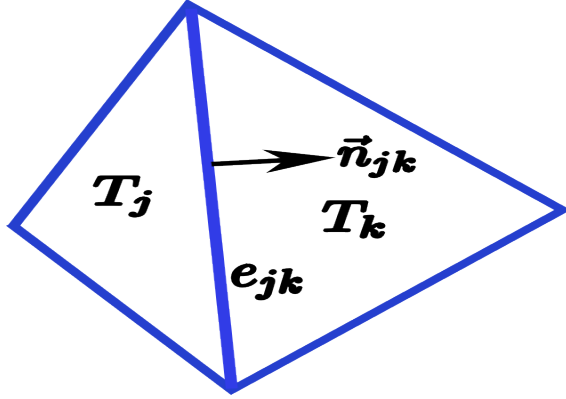


Figure 4: 2D mesh showing two neighbour cells, T_j and T_k , the edge e_{jk} between them and the normal vector \vec{n}_{jk}

In this section, we present the scheme for the flood flow model, (51). Let Ω_h^{2D} be a mesh of the floodplains and $T_j, T_k \in \Omega_h^{2D}$ are two neighbour cells in Ω_h^{2D} , see figure 4. Let e_{jk} be the edge between T_j and T_k , and \vec{n}_{jk} be the unit vector normal outwards to T_j . Furthermore, let $|T_j|$ and $|e_{jk}|$ be the area of T_j and length of e_{jk} respectively and let \mathcal{E}_j be the set of all edges of T_j . And let $\Pi_j^n = (H_j^n, q_{x,j}^n, q_{y,j}^n)^T$ and $\Pi_k^n = (H_k^n, q_{x,k}^n, q_{y,k}^n)^T$ be the approximate cell averages of the true solution in T_j and T_k respectively, namely

$$\Pi_j^n = \frac{1}{|T_j|} \int_{T_j} \Pi(\vec{X}, t^n) d\vec{x} \quad (53)$$

and $z_{b,j}, z_{b,k}$ be the average bottom elevations in T_j, T_k respectively.

To update cell average in T_j , we consider the 2D hydrostatic reconstruction finite volume scheme [1] in the following. For any vector $\vec{n} = (n_x, n_y)^T$, define a rotation matrix, $T_{\vec{n}}$ and its inverse, $T_{\vec{n}}^{-1}$

by

$$T_{\vec{n}} = \begin{pmatrix} 1 & 0 & 0 \\ 0 & n_x & n_y \\ 0 & -n_y & n_x \end{pmatrix}, \quad T_{\vec{n}}^{-1} = \begin{pmatrix} 1 & 0 & 0 \\ 0 & n_x & -n_y \\ 0 & n_y & n_x \end{pmatrix}, \quad (54)$$

see [24].

Define the following cell interface reconstructed quantities:

$$\tilde{H}_p^n := \max(H_p^n + z_{b,p} - \max(z_{b,j}, z_{b,k})), \quad \widetilde{T_{\vec{n}_{jk}} \Pi_p^n} := \frac{\tilde{H}_p^n}{H_p^n} T_{\vec{n}_{jk}} \Pi_p^n, \quad p = j, k. \quad (55)$$

Also the source function,

$$S^{hrm}(H_j^n, \tilde{H}_j^n) := \begin{pmatrix} 0 \\ \frac{g}{2} ((H_j^n)^2 - (\tilde{H}_j^n)^2) \\ 0 \end{pmatrix}. \quad (56)$$

Then the hydrostatic reconstruction scheme for the flood model, (51) becomes:

$$\Pi_j^{n+1} = \Pi_j^n - \frac{\Delta t}{|T_j|} \sum_{e_{jk} \in \mathcal{E}_j} |e_{jk}| \left(T_{\vec{n}_{jk}}^{-1} \phi(T_{\vec{n}_{jk}} \widetilde{T_{\vec{n}_{jk}} \Pi_j^n}, T_{\vec{n}_{jk}} \widetilde{T_{\vec{n}_{jk}} \Pi_k^n}) + T_{\vec{n}_{jk}}^{-1} S^{hrm}(H_j^n, \tilde{H}_j^n) \right) + \Delta t S_b(\Pi_j^n), \quad (57)$$

where ϕ is any numerical flux function consistent with the 1D component, $F_1(\Pi)$ of the 2D flux, $F(\Pi)$. Here, we consider the HLL scheme [13], namely

$$\phi(\Pi_L, \Pi_R) = \begin{cases} F_1(\Pi_L), & \text{if } s_L \geq 0, \\ F_1^* := \frac{s_R F_1(\Pi_L) - s_L F_1(\Pi_R) + s_L s_R (\Pi_R - \Pi_L)}{s_R - s_L}, & \text{if } s_L \leq 0 \leq s_R, \\ F_1(\Pi_R), & \text{if } s_R \leq 0, \end{cases} \quad (58)$$

where s_L and s_R are estimates of the smallest and largest wave speeds in the solution of the associated 1D Riemann problem [24]. There are several choices for s_L, s_R [24, 23]. We use the ones given in [7] namely

$$s_L = \min_k \{\lambda_k(\Pi_L), \lambda_k(\Pi_R)\}, \quad s_R = \max_k \{\lambda_k(\Pi_L), \lambda_k(\Pi_R)\}, \quad (59)$$

where $\lambda_k, k = 1, \dots, M$, are the eigenvalues of the Jacobian matrix of the system.

3.2 Scheme for the Open Channel Flow Model without Exchange nor Coupling Terms

Here, we consider the conventional 1D open channel flow model, namely

$$\begin{aligned} \partial_t A + \partial_x Q &= 0, \\ \partial_t Q + \partial_x \left(\frac{Q^2}{A} \right) &= -gA \partial_x \bar{\eta} + gAS_f. \end{aligned} \quad (60)$$

where A and Q are the wetted cross sectional area and sectional averaged discharge for the full channel cross section; $S_f = \frac{Q|Q|}{K^2}$ is the channel friction slope, $K = \frac{A^{k_1}}{n^{pk_2}}$ is the conveyance, P is the wetted perimeter of channel cross-section, $k_1 = 5/3, k_2 = 2/3$ and n is the Manning coefficient [17, 20, 9, 14].

To approximate the solution of (60), we consider a mesh Ω_h^1 of the channel, see figure 5(a). Let $\{x_{i+1/2}\}_{i=1}^{N_{1Dcell}}$ be points in the 1D grid, Ω_h^1 and $K_i = (x_{i-1/2}, x_{i+1/2}), i = 1, 2, \dots, N_{1Dcell}$ be a cell centred at $x_i = (x_{i-1/2} + x_{i+1/2})/2$ in Ω_h^1 . Where N_{1Dcell} is the number of cells in the 1D grid. Let

$W(x, t) = (A(x, t), Q(x, t))^T$ be a vector of conserved quantities at point, x and time, t , then the cell average vector, $W_i^n = (A_i^n, Q_i^n)^T$ in cell K_i is defined as

$$W_i^n = \frac{1}{\Delta x_i} \int_{K_i} W(x, t^n) dx, \quad (61)$$

where $\Delta x_i = x_{i+1/2} - x_{i-1/2}$, $t^n = t^{n-1} + \Delta t$, and Δt is the time step. We consider the scheme of [18] as summarised in [17]. The scheme is based on the formulation of the St Venant model as presented in [9] and rewrites the model in the quasi-linear form:

$$\partial_t W + J(W, B) \partial_x W = s'(x, W), \quad (62)$$

where $W = (A, Q)^T$, the Jacobian matrix, J is given by

$$J(W, B) = \begin{pmatrix} 0 & 1 \\ c^2 - \underline{u}^2 & 2\underline{u} \end{pmatrix}, \quad \underline{u} = \frac{Q}{A}, c = \sqrt{g \frac{A}{B}}, \quad s'(x, W) = \begin{pmatrix} 0 \\ gA \left[S_o - S_f - \frac{dH}{dx} + \frac{1}{B} \frac{dA}{dx} \right] \end{pmatrix}, \quad (63)$$

B is the top width at the free-surface, H is the water depth from the 1D bottom elevation, $Z_b(x)$ to the flat free-surface, $\bar{\eta}$ and $S_o = -\frac{dZ_b}{dx}$ is the negative of channel bed slope. Details about this formulation can be found in [17]. The eigenvalues and eigenvectors of $J(W, B)$ are

$$\lambda_1(W, B) = \underline{u} - c, \quad \lambda_2(W, B) = \underline{u} + c \quad \text{and} \quad \mathbf{e}_1(W, B) = (1, \lambda_1(W, B))^T, \quad \mathbf{e}_2(W, B) = (1, \lambda_2(W, B))^T$$

respectively.

Define the Roe averages:

$$\hat{A}_{i+1/2} = \frac{1}{2}(A_i + A_{i+1}) \quad \hat{\underline{u}}_{i+1/2} = \frac{\sqrt{A_i} \underline{u}_i + \sqrt{A_{i+1}} \underline{u}_{i+1}}{\sqrt{A_i} + \sqrt{A_{i+1}}}, \quad \hat{W}_{i+1/2} = \begin{pmatrix} \hat{A}_{i+1/2} \\ \hat{\underline{u}}_{i+1/2} \end{pmatrix}. \quad (64)$$

$$\hat{B}_{i+1/2} = \frac{1}{2}(B_i + B_{i+1}) \quad \hat{H}_{i+1/2} = \left(\frac{\hat{A}}{\hat{B}} \right)_{i+1/2}, \quad \hat{c}_{i+1/2} = \sqrt{g \hat{H}_{i+1/2}}. \quad (65)$$

$$(\hat{S}_o)_{i+1/2} = \frac{Z_{b,i+1} - Z_{b,i}}{x_{i+1} - x_i}, \quad (\hat{S}_f)_{i+1/2} = S_f(\hat{v}_{i+1/2}). \quad (66)$$

Define $(\Delta p)_{i+1/2} = p_{i+1} - p_i$ for any quantity, p . Then, define

$$(\hat{\alpha}_1)_{i+1/2} = \left[\frac{\hat{\lambda}_2 \Delta A - \Delta Q}{2\hat{c}} \right]_{i+1/2}, \quad (\hat{\alpha}_2)_{i+1/2} = \left[\frac{-\hat{\lambda}_1 \Delta A + \Delta Q}{2\hat{c}} \right]_{i+1/2}. \quad (67)$$

$$(\hat{\beta}_1)_{i+1/2} = \left(-g \frac{\hat{A}}{2\hat{c}} \left[(\hat{S}_0 - \hat{S}_f) \Delta x - \Delta H + \frac{1}{\hat{B}} \Delta A \right] \right)_{i+1/2}, \quad (\hat{\beta}_2)_{i+1/2} = -(\hat{\beta}_1)_{i+1/2}. \quad (68)$$

The Roe averaged eigenvalues and eigenvectors are

$$(\hat{\lambda}_m)_{i+1/2} := \lambda_m(\hat{W}_{i+1/2}, \hat{B}_{i+1/2}), \quad (\hat{\mathbf{e}}_m)_{i+1/2} := \mathbf{e}_m(\hat{W}_{i+1/2}, \hat{B}_{i+1/2}), \quad m = 1, 2. \quad (69)$$

The artificial viscosity (entropy fix), \hat{v} to correct the entropy problem associated with the Roe method [17] is given by

$$(\hat{v}_m)_{i+1/2} = \begin{cases} \frac{1}{4} [(\lambda_m)_{i+1} - (\lambda_m)_i], & \text{if } (\lambda_m)_i < 0 < (\lambda_m)_{i+1}, \\ 0, & \text{else} \end{cases}, \quad m = 1, 2. \quad (70)$$

Hence, the numerical scheme of [17, 18] for the 1D channel model without coupling term, (??) is given by

$$\mathbf{W}_i^{n+1*} = \mathbf{W}_i^n - \frac{\Delta t}{\Delta x} \left[\sum_{m=1}^2 \left(\hat{\gamma}_m^+ \hat{\mathbf{e}}_m \right)_{i-1/2} + \sum_{m=1}^2 \left(\hat{\gamma}_m^- \hat{\mathbf{e}}_m \right)_{i+1/2} \right]^n, \quad (71)$$

where

$$\left(\hat{\gamma}_m^\pm \right)_{i+1/2} = \left[\frac{1}{2} [1 \pm \text{sgn}(\hat{\lambda})] \hat{\gamma} \pm \hat{v} \hat{\alpha} \right]_{m,i+1/2}, \quad \left(\hat{\gamma}_m \right)_{i+1/2} = \left(\hat{\lambda} \hat{\alpha} - \hat{\beta} \right)_{m,i+1/2}, \quad m = 1, 2. \quad (72)$$

4 Numerical Algorithm for the Coupled Channel Flow Models

In this section, we describe in detail the numerical schemes and algorithms to solve the two-layer models, (49) and (50) for the channel flow. The approach we propose follows three major steps, namely (i) step one involves distributing the given full 2D data among the lower and upper layers. (ii) Step two evolves each layer data to its update values. This step involves two stages - the stage one computes the sub-layer intermediate solutions and channel/floodplain flows interaction, while stage two computes the exchange terms and the update values for the sub-layers and (iii) step three assembles the update values of the layers to obtain the desired update value of the full 2D data.

4.1 Background

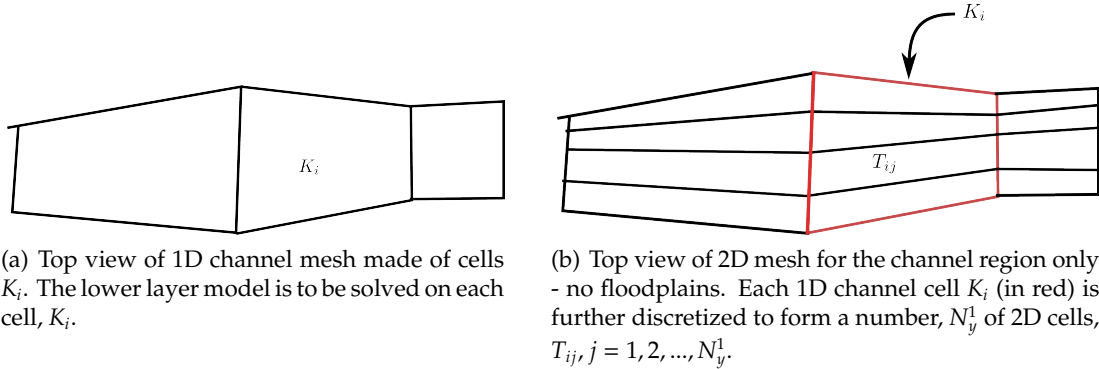


Figure 5: Mesh for the two sub-models.

Let $K_i = (x_{i-1/2}, x_{i+1/2}) \in \Omega_h^1$ be a cell in the 1D channel mesh Ω_h^1 , see figure 5(a). To consider the upper layer channel model, (50), we further discretize each channel cell K_i into 2D cells, T_{ij} , $j = 1, \dots, N_y^1$, see figure 5(b). This forms the channel upper layer 2D mesh Ω_h^2 , so that

$$\Omega_h^2 = \{T_{ij} : T_{ij} \in K_i \in \Omega_h^1, j = 1, \dots, N_y^1; i = 1, \dots, N_{1Dcells}\}. \quad (73)$$

See figures 6 and 7 for the layout of the grids in 3D view. We also discretize time as, t^n , $n = 1, 2, \dots, N^n$.

For the 1D cell, K_i , we define the following discrete channel quantities

$$\eta_i^\beta = z_b^w(x_i), \quad B_i = B(x_i, \eta_i^\beta), \quad A_{c,i} = A_c(x_i), \quad Z_{b,i} = Z_b(x_i), \quad \beta_i = \eta_i^\beta - Z_{b,i} \quad (74)$$

as the channel wall elevation, channel top width, critical area, 1D bed elevation, and channel depth respectively, at the center of 1D cell, K_i (see figure 8(a)). The discrete cell averages;

$$A_{1,i}^n \approx \frac{1}{\Delta x_i} \int_{x_{i-1/2}}^{x_{i+1/2}} A_1(x, t^n) dx, \quad Q_{1,i}^n \approx \frac{1}{\Delta x_i} \int_{x_{i-1/2}}^{x_{i+1/2}} Q_1(x, t^n) dx, \quad A_i^n \approx \frac{1}{\Delta x_i} \int_{x_{i-1/2}}^{x_{i+1/2}} A(x, t^n) dx \quad (75)$$

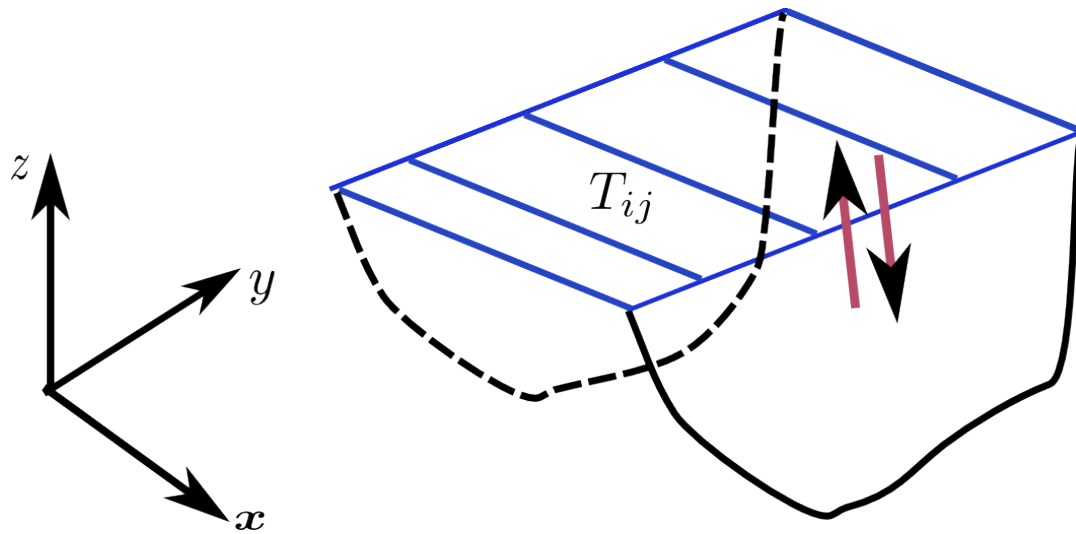


Figure 6: Three dimensional view of the channel meshes (without floodplain) showing a single 1D channel cell, K_i (the largest rectangle in blue) and the 2D channel cells, T_{ij} (the smaller blue rectangles). The channel bottom topography is shown in black. The arrows indicate the flow exchange between the two layers in the channel and it is computed during the second stage of the operator splitting method presented later.

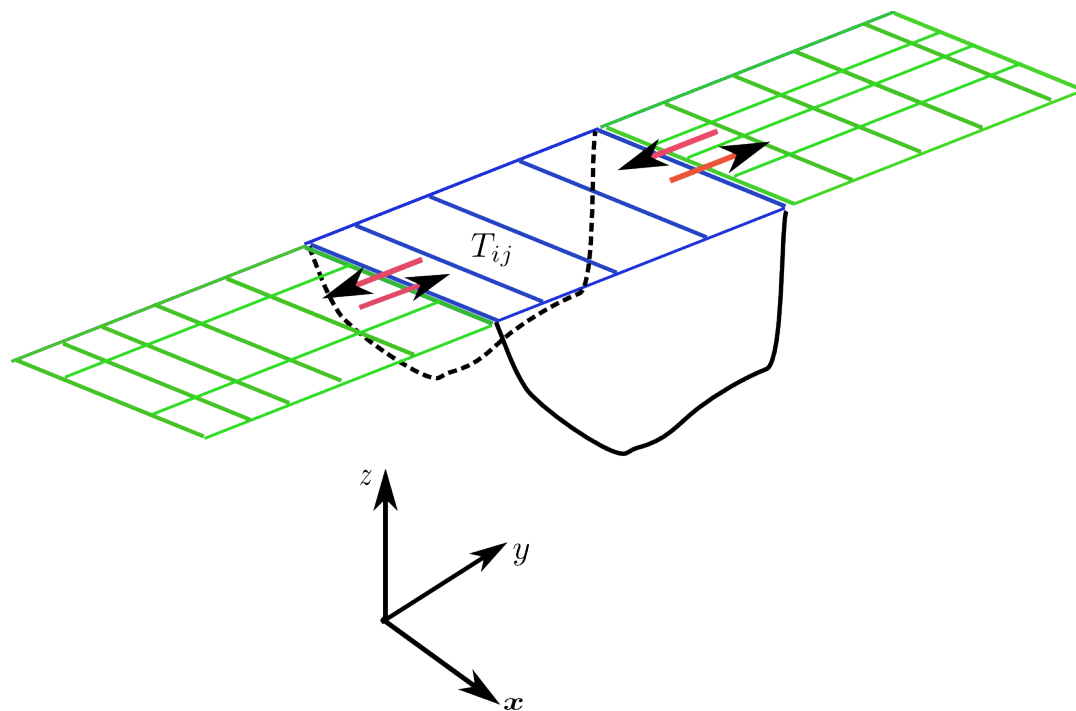


Figure 7: Three dimensional view of a single 1D channel cell, K_i (the largest rectangle in blue), the 2D channel cells, T_{ij} (the smaller blue rectangles) and the floodplain mesh (in green). The arrows indicate the flow exchange between the channel and the floodplain; these interactions are seamlessly computed by the 2D upper layer model while computing the intermediate solutions in the channel. The two layer model is not solved in the floodplain (green) mesh.

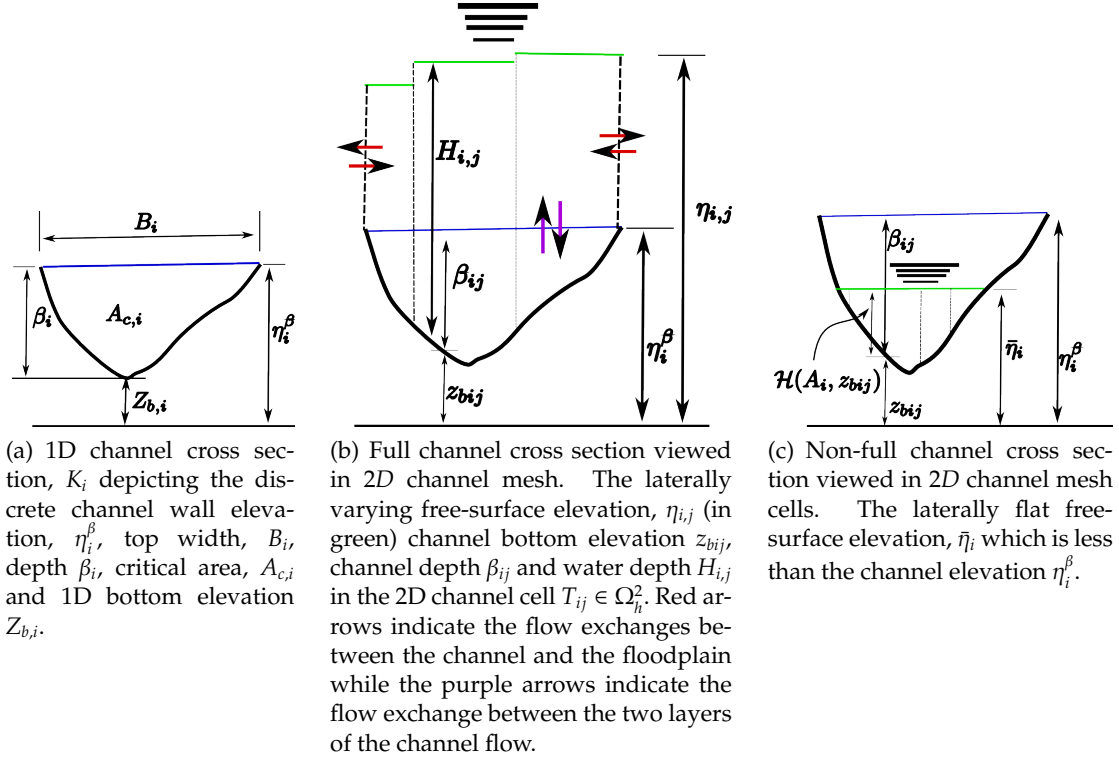


Figure 8: Discrete channel geometry in 1D channel cell (figure 8(a)) and the cross sectional view of the channel flow 2D channel cells when full (figure 8(b)) and non-full (figure 8(c)).

are for the wetted cross section and section-averaged discharge in lower layer and total wetted cross sectional area in cell, K_i .

For the associated 2D cells, T_{ij} in K_i , we define the following.

$$z_{bij} = z_b(\vec{X}_{ij}), \quad \beta_{ij} = \eta_i^\beta - z_{bij} \quad (76)$$

being the bed elevation and channel depth at the cell center, \vec{X}_{ij} of T_{ij} , see figure 8(b). Note the identity, $Z_{bi} + \beta_i = z_{bij} + \beta_{ij} = \eta_i^\beta \quad \forall j = 1, \dots, Ny^1$. We also define the cell averages for the 2D upper layer;

$$h_{2,i,j}^n \approx \frac{1}{|T_{ij}|} \int_{T_{ij}} h_2(\vec{X}, t^n) dx dy, \quad \vec{q}_{2,i,j}^n \approx \frac{1}{|T_{ij}|} \int_{T_{ij}} \vec{q}_2(\vec{X}, t^n) dx dy, \quad (77)$$

where $\vec{q}_2 = (q_{2x}, q_{2y})^T$ and $|T_{ij}|$ is the size(area) of T_{ij} .

Finally, we also note the following,

$$H_{i,j}^n \approx \frac{1}{|T_{ij}|} \int_{T_{ij}} H(\vec{X}, t^n) dx dy, \quad \vec{q}_{i,j}^n \approx \frac{1}{|T_{ij}|} \int_{T_{ij}} \vec{q}(\vec{X}, t^n) dx dy \quad (78)$$

which are cell averages for the full 2D data (sum of lower and upper layer) in 2D cells, $T_{ij} \in \Omega_h^2$.

4.1.1 Notation For Total Wetted Cross-Section Area in K_i Given the Free Surface Elevations in $T_{ij}, j = 1, \dots, N_y^1$: Given that the lateral distribution of the free-surface elevation in the 2D cells, T_{ij} in K_i are $\eta_{i,1}^n, \eta_{i,2}^n, \dots, \eta_{i,N_y^1}^n$, then we denote the wetted cross sectional area, A_i^n in K_i by

$$\mathcal{A}(\eta_{i,1}^n, \eta_{i,2}^n, \dots, \eta_{i,N_y^1}^n) \quad (\equiv A_i^n). \quad (79)$$

So, the function,

$$\mathcal{A} : \mathbb{R}^{N_y^1} \rightarrow \mathbb{R} \quad (80)$$

takes the free-surface elevations in the 2D cells in K_i and returns the wetted cross sectional area in K_i (see figure 8(b)).

The function, \mathcal{A} has to be **known** from the channel geometry. For instance, if the channel is of rectangular cross-section - with a laterally constant bottom elevation, $z_{bij} = Z_{bi}$ for all j , then \mathcal{A} would be given by

$$\mathcal{A}(\eta_{i,1}^n, \eta_{i,2}^n, \dots, \eta_{i,N_y^1}^n) = \sum_j^{N_y^1} (\eta_{i,j}^n - Z_{bi}) \Delta y_{ij} = \sum_j^{N_y^1} H_{i,j}^n \Delta y_{ij}. \quad (81)$$

4.1.2 Water Depth in 2D Cell, $T_{ij} \in K_i$ Given the Total Wetted Cross-Sectional Area in K_i : Let A_i^n be the total wetted cross-sectional area in cross-section K_i and z_{bij} , the bottom elevation in the 2D cell, $T_{ij} \in K_i$, then we denote by $\mathcal{H}(A_i^n, z_{bij})$, the water depth in T_{ij} such that the free surface is laterally flat. That is, the function

$$\mathcal{H} : \mathbb{R}^2 \rightarrow \mathbb{R} \quad (82)$$

takes the wetted cross sectional area in K_i and the bottom elevation in a 2D cell $T_{ij} \in K_i$, then returns the water depth in T_{ij} (see figure 8(c)). For instance, the channel depth, β_{ij} corresponds to the total water depth in T_{ij} if the total wetted cross-sectional area is equal to the critical area, $A_{c,i}$, hence

$$\mathcal{H}(A_{c,i}, z_{bij}) = \beta_{ij}. \quad (83)$$

Remark 4.1 Note that the definition of the function, \mathcal{H} has to be given (from the geometry of the channel).

Next, we recall the 1D consistency assumption in discrete version.

Definition 4.1 (Discrete Consistency requirement) In line with the consistency requirement in definition 2.7, we say that the solution, $(H, q_x, q_y)_{i,j}^n$ at t^n satisfies a discrete consistency requirement, if $\exists j^* \in \{1, 2, \dots, N_y^1\}$ such that $\eta_{i,j^*}^n < \eta_i^\beta$, then

$$\eta_{i,j}^n = \bar{\eta}_i^n < \eta_i^\beta \quad \forall j \in \{1, 2, \dots, N_y^1\}. \quad (84)$$

We will later show that if the initial data satisfies this discrete consistency requirement, then the requirement is satisfied for all time. In the next section, we begin with the first step of the numerical implementation process, namely to distribute a given full 2D data, $(H, \vec{q})_{ij}^n$ among the two layers.

4.2 Step 1 : Distribution of Full 2D data into two-layer data

Given the full 2D data, $(H, q_x, q_y)_{i,j}^n$ and z_{bij} in the 2D grid, Ω_h^2 , we distribute it among the two layers as follows. Define

$$\eta_{i,j}^n = H_{i,j}^n + z_{bij}, \quad u_{i,j}^n = \frac{q_{x,i,j}^n}{H_{i,j}^n}, \quad (85)$$

$$\bar{\eta}_i^n = \frac{1}{N_y^1} \sum_j \eta_{i,j}^n, \quad (86)$$

$$h_{1,i,j}^n = \min(H_{i,j}^n, \beta_{ij}), \quad q_{1x,i,j}^n = h_{1,i,j}^n u_{i,j}^n, \quad (87)$$

where $\eta_{i,j}^n$ and $u_{i,j}^n$ are the cell average free surface elevation and x-velocity respectively, in 2D cell. $\bar{\eta}_i^n$ is the averaged $\eta_{i,j}^n$ for all 2D cells in the 1D cell, K_i . $h_{1,i,j}^n$ and $q_{1x,i,j}^n$ are the lower layer (viewed as a 2D cell) height and x-discharge respectively. Having obtained the lower layer data $(h_{1,i,j}^n, q_{1x,i,j}^n)$ in 2D, we then use them to obtain the required 1D lower layer data for the 1D model.

4.2.1 Procedure For Lower Layer 1D Data We initialise the lower layer data as follows.

$$\begin{aligned} \eta_{1,i}^n &:= \min(\bar{\eta}_i^n, \eta_i^\beta) = \min(\eta_{1,i}^n, \eta_i^\beta) \quad (\text{by definition 4.1}). \\ A_{1,i}^n &= \mathcal{A}(\eta_{1,i}^n, \eta_{1,i}^n, \dots, \eta_{1,i}^n), \\ Q_{1,i}^n &= \sum_{j=1}^{N_y^1} q_{1x,i,j}^n \Delta y_{i,j}, \end{aligned} \quad (88)$$

where $\Delta y_{i,j}$ is the lateral width of $T_{i,j} \in K_i$.

4.2.2 Procedure For Upper Layer Data

$$\begin{aligned} h_{2,i,j}^n &= H_{i,j}^n - h_{1,i,j}^n \\ q_{2x,i,j}^n &= h_{2,i,j}^n u_{i,j}^n \\ q_{2y,i,j}^n &= h_{2,i,j}^n v_{i,j}^n \end{aligned} \quad (89)$$

where $v_{i,j}^n = \frac{q_{y,i,j}^n}{H_{i,j}^n}$. Having obtained the current time level data for each layer, we now use them to update each layer models in the next section, which is the second step of the algorithm.

4.3 Step 2 : Operator Splitting Method For Sub-Layer Models

We now solve the two layer channel models, (49), (50) in two stages. In stage one, we solve the models without the exchange terms and compute the lateral fluxes between the channel and floodplains (see figures 7 and 8(b)). This stage leads to the *intermediate solutions*. In the second stage, we compute the exchange terms to resolve the flow exchange between the two layers and update each layer data.

4.3.1 Step 2, stage 1: Sub-layers' intermediate solutions and channel/floodplain interaction: Let $(A_{1,i}, Q_{1,i})^{n+1*}$ be the approximate solution of the 1D lower layer model, (49) without exchange terms, namely

$$\begin{aligned} \partial_t A_1 + \partial_x Q_1 &= 0, \\ \partial_t Q_1 + \partial_x Q_1^2 / A_1 &= -g A_1 \partial_x \bar{\eta}, \end{aligned} \quad (90)$$

given the initial data, $(A_{1,i}, Q_{1,i})^n$. Also, let $(h_2, \vec{q}_2)_{i,j}^{n+1*}$ be the approximate solution of the upper layer 2D models, (50) without exchange terms, namely

$$\begin{aligned} \partial_t h_2 + \nabla \cdot \vec{q}_2 &= 0, \\ \partial_t \vec{q}_2 + \nabla \cdot F^q(h_2, \vec{q}_2) &= -gh_2 \nabla(z_b + h_1), \end{aligned} \quad (91)$$

given the initial data $(h_2, \vec{q}_2)_{i,j}^n$.

We call the solutions of (90) and (91), namely $(A_{1,i}, Q_{1,i})^{n+1*}$ and $(h_2, \vec{q}_2)_{i,j}^{n+1*}$, the *intermediate solutions*. At the moment, we assume that they (*the intermediate solutions*) have been obtained using an appropriate PDE solver. We postpone their solution methods to section 4.5. Note that solving (91) involves the computation of the lateral fluxes between the channel and the floodplains, hence the intermediate solution, $(h_2, \vec{q}_2)_{i,j}^{n+1*}$ accounts for the channel/floodplain flow interaction.

4.3.2 Step2, stage 2: Sub-layers' Exchange and Update Given the intermediate solutions, $(A_{1,i}, Q_{1,i})^{n+1*}$ and $(h_2, \vec{q}_2)_{i,j}^{n+1*}$, then the approximate solution of the 1D lower layer model including the exchange terms, (49) is the approximate solution of the system

$$\begin{aligned} \partial_t A_{1,i} &= - \int S dy, \\ \partial_t Q_{1,i} &= - \int u_{\eta_1} S dy, \end{aligned} \quad (92)$$

with the initial data, $(A_{1,i}, Q_{1,i})^{n+1*}$; and the approximate solution of the 2D models, (50) including the exchange terms is the approximate solution of the system

$$\begin{aligned} \partial_t h_{2,i,j} &= S, \\ \partial_t \vec{q}_{2,i,j} &= \vec{u}_{\eta_1} S, \end{aligned} \quad (93)$$

with the initial data, $(h_2, \vec{q}_2)_{i,j}^{n+1*}$.

Then using forward Euler time discretization, we approximate the solution of (92) and (93) as

$$\begin{aligned} A_{1,i}^{n+1} &= A_{1,i}^{n+1*} - S_i^A \Delta t, \\ Q_{1,i}^{n+1} &= Q_{1,i}^{n+1*} - S_i^Q \Delta t, \end{aligned} \quad (94)$$

and

$$\begin{aligned} h_{2,i,j}^{n+1} &= h_{2,i,j}^{n+1*} + S_{i,j} \Delta t, \\ \vec{q}_{2,i,j}^{n+1} &= \vec{q}_{2,i,j}^{n+1*} + \vec{u}_{\eta_1,i,j} S_{i,j} \Delta t, \end{aligned} \quad (95)$$

respectively, where

$$S_{i,j} \approx S|_{T_{i,j}}, \quad \vec{u}_{\eta_1,i,j} \approx \vec{u}_{\eta_1} \Big|_{T_{i,j}}, \quad S_i^A \approx \int_{K_i} S dy \quad \text{and} \quad S_i^Q \approx \int_{K_i} u_{\eta_1} S dy.$$

To complete the description of the scheme, we need to define the exchange terms and interface velocities; $S_{i,j}$, $\vec{u}_{\eta_1,i,j}$, S_i^A and S_i^Q . But there are no equations for these terms. However they can be determined by respecting the following conditions :

- (i) Conservation of mass and momentum.
- (ii) Discrete version of (37).
- (iii) Discrete consistency requirement (definition 4.1) of the resulting solution and
- (iv) And non-negativity of water heights.

The above conditions allow to first obtain the heights, hence the exchange terms, then the interface velocities are calculated.

Lower Layer Area: For global conservation, the total mass/momentum leaving one layer must equal the mass/momentum entering the other layer. Hence we assume the following:

$$S_i^A = \sum_j S_{i,j} \Delta y_{ij} \text{ and } S_i^Q = \sum_j u_{\eta_{1,i,j}} S_{i,j} \Delta y_{ij}. \quad (96)$$

Recall

$$A_i^{n+1} = A_{1,i}^{n+1} + \sum_j h_{2,i,j}^{n+1} \Delta y_j. \quad (97)$$

Substituting the expressions for $A_{1,i}^{n+1}$ and $h_{2,i,j}^{n+1}$ in (94) and (95) into (97), making use of the first conservation property, (96), then (97) gives

$$A_i^{n+1} = A_{1,i}^{n+1*} + \sum_j h_{2,i,j}^{n+1*} \Delta y_{ij}. \quad (98)$$

This explicitly gives the total wetted area, A_i^{n+1} directly from the intermediate solutions ($n+1^*$ values). Then, the discrete version of (37) gives

$$A_{1,i}^{n+1} = \min\left(A_i^{n+1}, A_{c,i}\right). \quad (99)$$

Upper Layer Heights: To compute the upper layer heights, we use the definition of $A_{1,i}^{n+1}$ in (99) alongside the relations (97) and (98). Before we continue, let's define the following notations, $A_{2,i}^{n+1*} := \sum_j h_{2,i,j}^{n+1*} \Delta y_{ij}$ and $A_{2,i}^{n+1} := \sum_j h_{2,i,j}^{n+1} \Delta y_{ij}$. We consider the following two cases based on the solution of $A_{1,i}^{n+1}$ in (99).

4.3.3 Case 1 : If $A_{1,i}^{n+1} = A_i^{n+1}$ (Lower Layer at t^{n+1} not full) Then by (97), we have $\sum_j h_{2,i,j}^{n+1} \Delta y_{ij} = A_i^{n+1} - A_{1,i}^{n+1} = 0$. Since $h_{2,i,j}^{n+1} \geq 0$, hence

$$h_{2,i,j}^{n+1} = 0. \quad (100)$$

4.3.4 Case 2 : If $A_{1,i}^{n+1} = A_{c,i}$ (Lower Layer at t^{n+1} full) Then, subtracting (98) from (97) gives

$$A_{2,i}^{n+1} = A_{2,i}^{n+1*} + \left(A_{1,i}^{n+1*} - A_{c,i}\right), \quad (101)$$

and consider two further cases.

4.3.5 Case 2a : If $A_{1,i}^{n+1*} - A_{c,i} \geq 0$ (Lower Layer full at intermediate state, t^{n+1*}) Then $A_{2,i}^{n+1} \geq A_{2,i}^{n+1*}$ by an amount $A_{2,i}^{n+1*} := A_{1,i}^{n+1*} - A_{c,i} \geq 0$, so we add the constant excess height, $h_{2,i,j}^{n+1*} = A_{2,i}^{n+1*} / B_i$ to the intermediate solution $h_{2,i,j}^{n+1*}$, namely

$$h_{2,i,j}^{n+1} = h_{2,i,j}^{n+1*} + \frac{A_{2,i}^{n+1*}}{B_i}. \quad (102)$$

4.3.6 Case 2b : If $A_{1,i}^{n+1*} - A_{c,i} < 0$ (Lower Layer not full at intermediate state, t^{n+1*}) Then $A_{2,i}^{n+1} < A_{2,i}^{n+1*}$ by the amount, $A_{gap,i}^{n+1*} = A_{c,i} - A_{1,i}^{n+1*} < 0$. Hence we remove $A_{gap,i}^{n+1*}$ from $A_{2,i}^{n+1*}$ using the following algorithm.

- initialize $h_{2,i,j}^{n+1} = h_{2,i,j}^{n+1*}$ for all T_{ij} .

- $h_{gap,i}^{n+1*} = \frac{A_{gap,i}^{n+1*}}{B_i}$, $TOL = 10^{-12}$.

- while($h_{gap,i}^{n+1*} > TOL$)

- i for all T_{ij}

- (a) $h_t = h_{2,i,j}^{n+1}$,

- (b) Reduce upper layer height by the gap height :

$$h_{2,i,j}^{n+1} = \max(0, h_{2,i,j}^{n+1} - h_{gap,i}^{n+1*}), \quad (103)$$

- (c) Remove area of reduced height from total gap area:

$$A_{gap,i}^{n+1*} = A_{gap,i}^{n+1*} - |h_{2,i,j}^{n+1} - h_t| \Delta y_{i,j},$$

- ii $h_{gap,i}^{n+1*} = \frac{A_{gap,i}^{n+1*}}{B_i}$.

Equations (100), (102) and (103) compute $h_{2,i,j}^{n+1}$ in $T_{ij} \in K_i$ for all three cases above.

Computing Exchange Terms and Interface Velocity: Having computed $h_{2,i,j}^{n+1}$, we now compute the exchange terms, $S_{i,j}$ using the first equation in (95), hence

$$S_{i,j} = \frac{h_{2,i,j}^{n+1} - h_{2,i,j}^{n+1*}}{\Delta t}. \quad (104)$$

Next, we compute the interface velocity, $\vec{u}_{\eta_{1,i,j}}$. As proposed for multilayer systems in [3], if water moves from lower layer to upper layer ($S_{i,j} > 0$), then the interface velocity, $\vec{u}_{\eta_{1,i,j}}$ is that of the lower layer. But if the reverse is the case ($S_{i,j} \leq 0$), then $\vec{u}_{\eta_{1,i,j}}$ is that of the upper layer. Hence we define

$$\vec{u}_{\eta_{1,i,j}} = \begin{cases} \vec{u}_{2,i,j}^{n+1*} = \frac{\vec{q}_{2y,i,j}^{n+1*}}{h_{2,i,j}^{n+1*}}, & \text{if } S_{i,j} \leq 0, \\ (u_{1,i}^{n+1*}, 0)^T = \left(\frac{Q_{1,i}^{n+1*}}{A_{1,i}^{n+1*}}, 0 \right)^T, & \text{if } S_{i,j} > 0. \end{cases} \quad (105)$$

Discharges: With the above definitions for exchange terms and interface velocity, then the upper layer discharge $q_{2,i,j}^{n+1}$ in (95) is completely determined. The use of conservation property (second equation in (96)) enables to compute S_i^Q from the 2D exchange terms and interface velocity, so the lower layer section averaged discharge, $Q_{1,i}^{n+1}$ in (94) is also completely computed. Hence, the discharges for both layers are obtained. Therefore, we now have $(A_{1,i}, Q_{1,i})^{n+1}$, and $(h_{2,i}, \vec{q}_{2,i})_{i,j}^{n+1}$. With these results, we update the full 2D data, $(H_{i,j}, \vec{q}_{i,j})^{n+1}$ in the next section which is the third and last step.

4.4 Step 3: Updating full 2D data $H_{i,j}^{n+1}$, $q_{x,i,j}^{n+1}$ and $q_{y,i,j}^{n+1}$ for $T_{i,j} \in K_i$

The full water depth, $H_{i,j}^{n+1}$ is given by

$$H_{i,j}^{n+1} = h_{1,i,j}^{n+1} + h_{2,i,j}^{n+1}, \quad (106)$$

where

$$h_{1,i,j}^{n+1} = \mathcal{H}(A_{1,i}^{n+1}, z_{bij}). \quad (107)$$

The full 2D x-discharge is computed as

$$\begin{aligned} q_{x,i,j}^{n+1} &:= q_{1x,i,j}^{n+1} + q_{2x,i,j}^{n+1} \\ &= h_{1,i,j}^{n+1} \frac{Q_{1,i}^{n+1}}{A_{1,i}^{n+1}} + q_{2x,i,j}^{n+1}. \end{aligned} \quad (108)$$

Finally, the lateral discharge is computed as follows :

$$q_{y,i,j}^{n+1} = H_{i,j}^{n+1} v_{i,j}^{n+1}, \quad (109)$$

where

$$v_{i,j}^{n+1} := v_{2,i,j}^{n+1} = \begin{cases} \frac{q_{2y,i,j}^{n+1} + v_{n1,i,j} S_{i,j} \Delta t}{h_{2,i,j}^{n+1}}, & \text{if } h_{2,i,j}^{n+1} > 0, \\ 0, & \text{else.} \end{cases} \quad (110)$$

This completes the numerical algorithm for the channel flow. As mentioned above, the scheme for the floodplain flow is the 2D solver presented in section ?? . At channel/floodplain interface, the lateral fluxes are effortlessly computed since the channel 2D cell, $T_{ij} \in K_i \in \Omega_h^1$ has the complete 2D data, $(H_{i,j}, \vec{q}_{i,j})^n$. This is not the case for most existing methods because the channel lateral discharge is not usually available. In the VCM, the fluxes between the floodplain and channel are taken into account in the first stage of operator splitting step where the intermediate solutions are computed. Figures 9 and 10 are the flow charts for the VCM algorithm.

4.5 Finite Volume Methods for the Intermediate Solutions

We now propose solution methods for the models, (90) and (91). Let us emphasize that the choice of method of solution for these models, is open to any appropriate PDE solver. In the following subsections, we adapt existing finite volume methods for this purpose.

4.5.1 Solution of Upper Layer Model without Exchange Terms As can be seen in the 2D model, (91) it can be interpreted as a 2D shallow water equation with topography, $z_b(\vec{X}) + h_1(\vec{X}, t)$ referred to as the apparent topography in [6, 7]. Therefore, we propose the following apparent topography hydrostatic reconstruction scheme [1, 6, 7]

$$U_{2,i,j}^{n+1*} = U_{2,i,j}^n - \frac{\Delta t}{|T_{ij}|} \sum_{e_k \in \mathcal{E}_{ij}} |e_k| \left(\phi^{2D}(\tilde{U}_{2,k,L}^n, \tilde{U}_{2,k,R}^n, \vec{n}_k) + s(h_{2,i,j}^n, \tilde{h}_{2,k,L}^n, \vec{n}_k) \right), \quad (111)$$

where e_k is k -th edge of T_{ij} , with size, $|e_k|$ and outward unit normal, \vec{n}_k . L and R indicate the cells at left and right of the edge, \mathcal{E}_{ij} is the set of all edges of T_{ij} and $U_{2,i,j}^{n+1*} = (h_{2,i,j}^{n+1*}, \vec{q}_{2,i,j}^{n+1*})^T$ is the upper

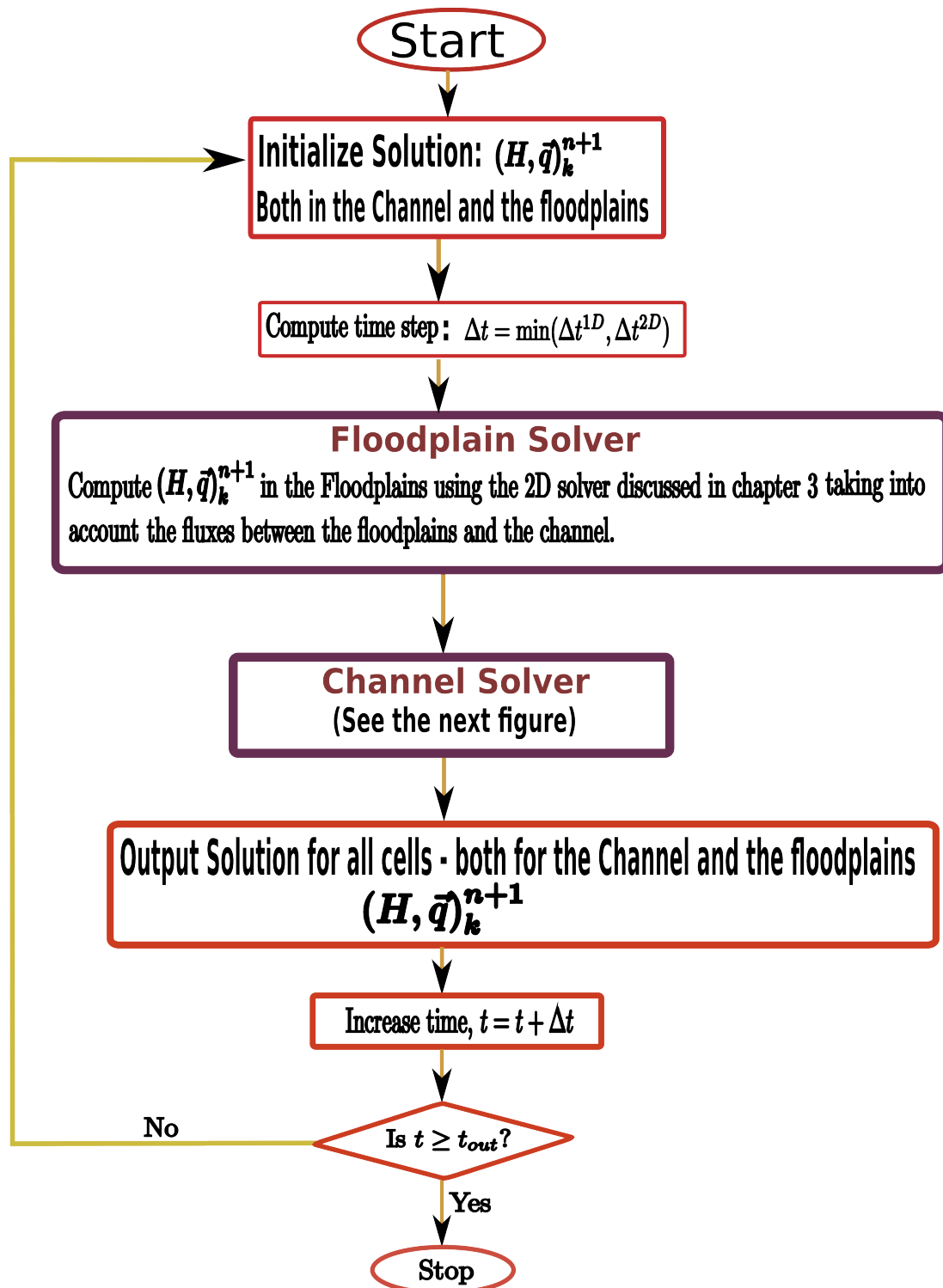


Figure 9: Flow chart for the VCM depicting the floodplain flow solver and the channel flow solver. The details of the channel solver is illustrated in figure 10.

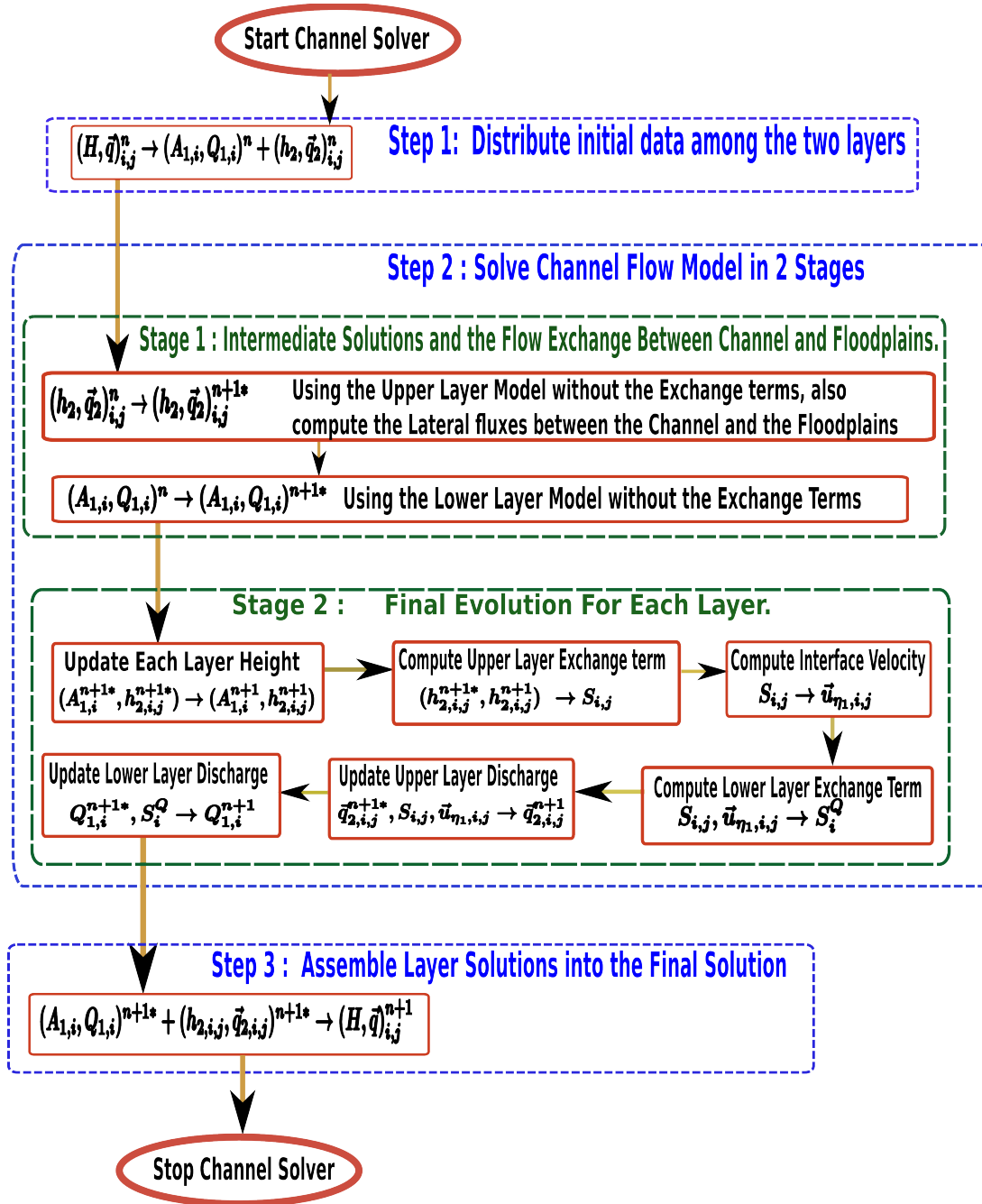


Figure 10: Details of the channel solver part in the flow chart of the VCM (figure 9). It depicts the three-step channel flow solver which implements the two-layer coupled models, (49), (50). It also shows the two stages to solve (step 2) the channel models. Step 2, stage 1 computes the intermediate solutions and the lateral fluxes between the channel and the floodplains, while step 2, stage 2 enforces the mass and momentum conservation to update each layer solution.

layer *intermediate solution* which is being computed. And

$$\begin{aligned}
\phi^{2D}(\tilde{U}_{2,k,L}^n, \tilde{U}_{2,k,R}^n, \vec{n}_k) &= T_{\vec{n}_k}^{-1} \phi(T_{\vec{n}_k} \tilde{U}_{2,k,L}^n, T_{\vec{n}_k} \tilde{U}_{2,k,L}^n), \\
s(h_{2,i,j}^n, \tilde{h}_{2,k,L}^n, \vec{n}_k) &= \frac{\delta}{2} \left(0, ([h_{2,i,j}^n]^2 - [\tilde{h}_{2,k,L}^n]^2) \vec{n}_k \right)^T, \\
\tilde{U}_{2,k,p}^n &= \frac{\tilde{h}_{2,k,p}^n}{h_{2,k,p}^n} U_{2,k,p}^n, \\
U_{2,i,j}^n &= (h_{2,i,j}^n, \vec{q}_{2,i,j}^n)^T, \\
U_{2,k,p}^n &= (h_{2,k,p}^n, \vec{q}_{2,k,p}^n)^T, \\
\tilde{h}_{2,k,p}^n &= \max(\eta_{k,p}^n - \eta_{1,k}^{n*}, 0), \\
\eta_{k,p}^n &= \eta_{1,k,p}^n + h_{2,k,p}^n, \\
p &= L, R.
\end{aligned} \tag{112}$$

k is the edge number.

$$\begin{aligned}
\eta_{1,k,p}^n &= z_{b,k,p} + h_{1,k,p}^n \quad (\text{The apparent topography on side } p = L, R), \\
\eta_{1,k}^{n*} &= \max(\eta_{1,k,R}^n, \eta_{1,k,L}^n).
\end{aligned} \tag{113}$$

The quantities, $z_{b,k,p}$, $h_{1,k,p}^n$, $\eta_{1,k,p}^n$ and $\eta_{k,p}^n$ are respectively, the bottom elevation, water depth of lower layer, top elevation of lower layer, and free-surface elevation of 2D cell on side P , ($P = L, R$) of the k -th edge of cell, T_{ij} .

Since the hydrostatic reconstruction method is mass conservative, [2, 1] and the 2D model, (91) does not introduce any source term to the height equation, then the scheme (111) is conservative. We state and prove a theorem below to show that this scheme, like the standard hydrostatic reconstruction [1] method, preserves well-balance of lake at rest,

4.5.2 Solution of Lower Layer Model without Exchange Terms Recall that if the channel is full, then the lower layer top elevation ($z = \eta_1(x, t) = z_b^w(x)$) is different from the free-surface elevation, ($z = \bar{\eta}(x, t)$) appearing in the lower layer 1D model. In this case, the top of the lower layer will not generally be constant (in x) even when the free-surface is constant (in x). This leads to difficulty in deriving a well-balance method for the lower layer model. In order to tackle this problem, we propose to approximate the solution of the lower layer model in the following way. Consider the two systems of equations

$$\partial_t \begin{pmatrix} A \\ Q \end{pmatrix} = -\partial_x \begin{pmatrix} Q \\ \frac{Q^2}{A} \end{pmatrix} - \begin{pmatrix} 0 \\ gA\partial_x \bar{\eta} \end{pmatrix} + \Phi(x, t) \tag{114}$$

and

$$\partial_t \begin{pmatrix} A_2 \\ Q_2 \end{pmatrix} = -\partial_x \begin{pmatrix} Q_2 \\ \frac{Q_2^2}{A_2} \end{pmatrix} - \begin{pmatrix} 0 \\ gA_2\partial_x \bar{\eta} \end{pmatrix} + \Phi(x, t). \tag{115}$$

The system, (114) is the 1D model for the full channel flow and $\Phi(x, t) = (\Phi^A(x, t), \Phi^Q(x, t))^T$ is a lateral coupling term (see [20, 21]). The system, (115) is a 1D model for the upper layer obtained by integrating the upper layer 2D model and considering a laterally constant free surface. Subtracting (115) from (114) gives

$$\partial_t \begin{pmatrix} A - A_2 \\ Q - Q_2 \end{pmatrix} = -\partial_x \begin{pmatrix} Q - Q_2 \\ \frac{(Q - Q_2)^2}{A - A_2} \end{pmatrix} - \begin{pmatrix} 0 \\ g(A - A_2)\partial_x \bar{\eta} \end{pmatrix} + \partial_x \left(\frac{AA_2}{A - A_2} (\bar{u} - \bar{u}_2)^2 \right),$$

where $\bar{u} = \frac{Q}{A}$ and $\bar{u}_2 = \frac{Q_2}{A_2}$. Using the fact that the vertical variation of velocity is negligible, hence $(\bar{u} - \bar{u}_2)^2 \approx 0$, we have

$$\partial_t \begin{pmatrix} A_1 \\ Q_1 \end{pmatrix} \approx \partial_t \begin{pmatrix} A - A_2 \\ Q - Q_2 \end{pmatrix}, \quad (116)$$

since

$$\partial_t \begin{pmatrix} A_1 \\ Q_1 \end{pmatrix} = -\partial_x \begin{pmatrix} Q_1 \\ \frac{Q_1^2}{A_1} \end{pmatrix} - \begin{pmatrix} 0 \\ gA_1 \partial_x \bar{\eta} \end{pmatrix}.$$

Hence, from (116), we propose to approximate the solution of the lower layer model, (90) as

$$\begin{pmatrix} A_{1,i} \\ Q_{1,i} \end{pmatrix}^{n+1*} = \begin{pmatrix} A_i \\ Q_i \end{pmatrix}^{n+1*} - \begin{pmatrix} A_{2,i} \\ Q_{2,i} \end{pmatrix}^{n+1*}, \quad (117)$$

where $(A_i^{n+1*}, Q_i^{n+1*})^T$ is the approximate solution of the full layer 1D model, (114) solved with any known method and $(A_{2,i}^{n+1*}, Q_{2,i}^{n+1*})^T \approx \sum_j \left(h_{2,i,j}^{n+1*}, q_{2x,i,j}^{n+1*} \right)^T \Delta y_{i,j}$ is obtained from the 2D solution, (111). So we do not need to solve (115), rather we approximate its solution with those of the 2D upper layer. We use the scheme of [17] presented in section 3.2, for the solution of the model, (114), see [20, 21] for the details.

In summary, what we have proposed for the lower layer model, is to solve (114), use the solution of (111), then apply (117) to obtain the lower layer intermediate solution. It is important to reiterate that this approach is just one possible way of solving the lower layer model, (90). There might be other ways of solving this model and still achieve the desired properties. In the following, we prove that if the underlying solver for (114) is well-balanced and mass conservative, then the lower layer scheme, (117) is also well-balanced and mass conservative.

5 Properties of the Scheme

We now consider some properties of the scheme proposed above.

Definition 5.1 (Consistency of Distribution Operation) We require a distribution operation (step 1) such as the one in section 4.2 to be **consistent** in the sense that whenever the channel is not full ($H_{i,j}^n \leq \beta_{ij} \quad \forall T_{ij} \in K_i$), then the following conditions must hold:

- i $h_{2i,j}^n, q_{2xi,j}^n$ and $q_{2yi,j}^n$ each equal zero $\forall T_{ij} \in K_i$;
- ii The lower layer area, $A_{1,i}^n$ must correspond to total water in cross-section. That is, $A_{1,i}^n = \mathcal{A}(\eta_{i,1}^n, \eta_{i,2}^n, \dots, \eta_{i,N_y}^n)$ ($= \sum_j H_{i,j}^n \Delta y_j$ if channel is locally rectangular).

These ensure that we do not solve two-layer problem when the flow is actually one-layer (not full) and in such case, the lower layer must account for the total water in the cross-section. This is the self-adaptive nature of the scheme.

Definition 5.2 (No-Numerical Flooding Property) In order to satisfy the no-numerical flooding property, the solution of the scheme, $(H_{i,j}, q_{xi,j}, q_{yi,j})^{n+1}$ must satisfy the following conditions:

- i $(\beta_{ij} - h_{1i,j}^{n+1})h_{2i,j}^{n+1} = 0 \quad \forall T_{ij} \in K_i$; (118)
- ii If $h_{2i,j}^{n+1} = 0$, then (a) $q_{2x,i,j}^{n+1} = 0$ (b) $u_{i,j}^{n+1} = \frac{Q_{1,i}^{n+1}}{A_{1,i}^{n+1}}$ (which is constant laterally) and (c) $q_{y,i,j}^{n+1} = 0$;

iii If $\exists j^* \in \{1, 2, \dots, N_y^1\} \mid \eta_{i,j^*}^{n+1} < \eta_i^\beta$, then $\eta_{i,j^*}^{n+1} = \eta_{i,j^*}^{n+1} \forall j$.

This ensures that the solution at $t^n + 1$ satisfies the discrete consistency requirement (see definition 4.1).

Condition (i) means that lower layer is either full ($h_{1,i,j} = \beta_{i,j}$) or upper layer is dry $h_{2,i,j} = 0$. In other words, there shouldn't be gap between the two layers. This way, water would not overflow when the channel is not yet full. Condition (ii) states that if upper layer is dry, then the flow must be 1D. That is, if upper layer is dry, then its velocities and discharges must be zero. And the full layer data must be laterally uniform. Condition (iii) means that if channel is not full, then the free-surface must be flat (equal) in lateral direction. This is the discrete consistency requirement (definition 4.1) on the solution at t^{n+1} .

In addition, we also prove that the scheme is well-balanced and conservative under suitable conditions on the intermediate solutions.

Theorem 5.1 (Consistency of Distribution Operation) *The distribution operation proposed in section 4.2 is consistent with the problem in the sense of definition 5.1.*

Proof: We need to prove (i) and (ii) in definition 5.1.

i) If the channel is not full, then

$$H_{i,j}^n \leq \beta_{ij}.$$

Hence, by (89), we have

$$h_{2,i,j}^n = H_{i,j}^n - \min(H_{i,j}, \beta_{ij}) = H_{i,j}^n - H_{i,j}^n = 0.$$

Consequently,

$$q_{2x,i,j}^n = q_{2y,i,j}^n = 0 \text{ by (89).}$$

ii)

$$H_{i,j}^n \leq \beta_{i,j} \Rightarrow z_{bij} + H_{i,j}^n \leq z_{bij} + \beta_{i,j} \Rightarrow \eta_{i,j}^n \leq \eta_i^\beta.$$

Hence, by discrete consistency (definition 4.1), we have

$$\bar{\eta}_i = \eta_{i,j}^n < \eta_i^\beta \forall j = 1, \dots, N_y^1.$$

By (88),

$$\eta_{1,i}^n := \min(\bar{\eta}_i, \eta_i^\beta) = \bar{\eta}_i = \eta_{i,j}^n \forall j = 1, \dots, N_y^1.$$

Hence,

$$A_{1,i}^n := \mathcal{A}(\eta_{1,i}^n, \eta_{1,i}^n, \dots, \eta_{1,i}^n) = \mathcal{A}(\eta_{i,1}^n, \eta_{i,2}^n, \dots, \eta_{i,N_y^1}^n) =: \text{total wetted area.}$$

□

Theorem 5.2 (No-Numerical Flooding Property) *The vertical coupling scheme as derived in (106), (108) and (109), preserves the no-numerical flooding property in the sense of definition 5.2.*

Proof:

i We prove (118) on case-by-case bases.

Case 1:

$$h_{2,i,j}^{n+1} = 0, \quad \text{see (100).}$$

Cases 2a and 2b :

$$A_{1,i}^{n+1} = A_{c,i} \Rightarrow h_{1,i,j}^{n+1} := \mathcal{H}(A_{1,i}^{n+1}, z_{bij}) = \mathcal{H}(A_{c,i}, z_{bij}) = \beta_{ij}.$$

Therefore,
 $h_{2,i,j}^{n+1} = 0$ or $h_{1,i,j}^{n+1} = \beta_{ij}$ in all cases. Hence,

$$(\beta_{ij} - h_{1,i,j}^{n+1})h_{2,i,j}^{n+1} = 0 \quad \forall T_{ij} \in K_i$$

as claimed.

ii Let $h_{2,i,j}^{n+1} = 0$, then

(a)

$$S_{i,j} = -\frac{h_{2,i,j}^{n+1*}}{\Delta t} < 0 \Rightarrow u_{\eta_{1,i,j}} = u_{2,i,j}^{n+1*} \Rightarrow u_{\eta_{1,i,j}} S_{i,j} \Delta t = q_{2x,i,j}^{n+1*} \Rightarrow q_{2x,i,j}^{n+1} = 0.$$

(b) Since $q_{2x,i,j}^{n+1} = 0$, then

$$q_{x,i,j}^{n+1} = h_{1,i,j}^{n+1} \frac{Q_{1,i}^{n+1}}{A_{1,i}^{n+1}} = \frac{Q_{1,i}^{n+1}}{A_{1,i}^{n+1}} H_{i,j}^{n+1} \text{ (because } h_{2,i,j}^{n+1} = 0 \text{)}.$$

Hence,

$$u_{i,j}^{n+1} := \frac{q_{x,i,j}^{n+1}}{H_{i,j}^{n+1}} = \frac{Q_{1,i}^{n+1}}{A_{1,i}^{n+1}} \text{ (which is constant in } j \text{)}.$$

(c)

$$v_{i,j}^{n+1} = 0 \text{ (see(110))} \Rightarrow q_{y,i,j}^{n+1} = 0.$$

iii Let there exist $j^* \in \{1, 2, \dots, N_y^1\}$ such that $\eta_{i,j^*}^{n+1} < \eta_i^\beta$, then this corresponds to case 1 in step 2 because cases 2a and 2b satisfy

$$A_{1,i}^{n+1} = A_{c,i} \Rightarrow \eta_{i,j}^{n+1} \geq \eta_i^\beta \forall j = 1, \dots, N_y^1.$$

Since, $\eta_{i,j^*}^{n+1} < \eta_i^\beta$ corresponds to case 1, then it satisfies

$$A_{1,i}^{n+1} = A_i^{n+1} \leq A_{c,i} \Rightarrow h_{2,i,j}^{n+1} = 0 \forall j.$$

So,

$$\eta_{i,j}^{n+1} := H_{i,j}^{n+1} + z_{bij} = h_{1,i,j}^{n+1} + z_{bij} = \eta_{1,i}^{n+1} \forall j = 1, \dots, N_y^1.$$

That is,

$$\eta_{i,j}^{n+1} = \eta_{1,i}^{n+1} = \eta_{i,j^*}^{n+1} \forall j = 1, \dots, N_y^1.$$

Hence the free surface is laterally flat. Therefore, the discrete consistency requirement (definition 4.1) holds at t^{n+1} . Therefore, the scheme satisfies the no-numerical flooding property.

□

Theorem 5.3 (Well-balance) *If the numerical schemes for the intermediate solutions, $(A_{1,i}^{n+1*}, Q_{1,i}^{n+1*})^T$ and $(h_{2,i,j}^{n+1*}, q_{2x,i,j}^{n+1*}, q_{2y,i,j}^{n+1*})^T$ are well-balanced, then the vertical coupling method, (106), (108) and (109), is well-balanced. This is true for any kind of well-balance, not only for lake at rest.*

Proof: Let the intermediate solutions be well-balanced, then

$$\begin{aligned} (A_{1,i}^{n+1*}, Q_{1,i}^{n+1*})^T &= (A_{1,i}^n, Q_{1,i}^n)^T, \\ (h_{2,i,j}^{n+1*}, q_{2x,i,j}^{n+1*}, q_{2y,i,j}^{n+1*})^T &= (h_{2,i,j}^n, q_{2x,i,j}^n, q_{2y,i,j}^n)^T. \end{aligned}$$

Recall that

$$\begin{aligned} A_{1,i}^n &= \min(A_i^n, A_{c,i}), \\ A_{1,i}^{n+1} &:= \min(A_i^{n+1}, A_{c,i}) = \min(A_{1,i}^{n+1*} + A_{2,i}^{n+1*}, A_{c,i}) \\ &= \min(A_{1,i}^n + A_{2,i}^n, A_{c,i}) \text{ (intermediate solutions are well-balanced)} \\ &= A_{1,i}^n. \end{aligned}$$

$$\text{Hence, } h_{1,i,j}^{n+1} = h_{1,i,j}^n.$$

Next, we show that $h_{2,i,j}^{n+1} = h_{2,i,j}^n$.

$$\begin{aligned} A_{2,i}^{n+1} &:= A_i^{n+1} - A_{1,i}^{n+1} = (A_{1,i}^{n+1*} + A_{2,i}^{n+1*}) - A_{1,i}^n \\ &= (A_{1,i}^n + A_{2,i}^{n+1*}) - A_{1,i}^n = A_{2,i}^{n+1*} \\ &= A_{2,i}^n \Rightarrow A_i^{n+1} = A_i^n. \end{aligned}$$

Case 1: $A_{1,i}^{n+1} = A_i^{n+1} < A_{c,i}$, that is

$$A_{1,i}^{n+1} = A_i^{n+1} = A_i^n < A_{c,i}.$$

But $A_i^n < A_{c,i} \Rightarrow h_{2,i,j}^n = 0$, that is

$$h_{2,i,j}^{n+1*} = h_{2,i,j}^n = 0.$$

Also,

$$A_i^{n+1} < A_{c,i} \Rightarrow h_{2,i,j}^{n+1} = 0 = h_{2,i,j}^n.$$

Cases 2a and 2b: $A_{1,i}^{n+1} = A_{c,i}$, that is

$$A_{1,i}^{n+1} = A_{1,i}^n = A_{1,i}^{n+1*} = A_{c,i}.$$

But

$$A_{1,i}^{n+1*} = A_{c,i} \Rightarrow A_{\text{excess},i}^{n+1*} = A_{\text{gap}}^{n+1*} = 0 \Rightarrow h_{\text{excess},i}^{n+1*} = h_{\text{gap}}^{n+1*} = 0.$$

Hence by (102) and (103), we have

$$h_{2,i,j}^{n+1} = h_{2,i,j}^{n+1*} = h_{2,i,j}^n.$$

Finally, we show that $(H, \vec{q}_2)_{i,j}^{n+1} = (H, \vec{q}_2)_{i,j}^{n+1}$.

$$\begin{aligned} &\Rightarrow H_{i,j}^{n+1} = h_{1,i,j}^n + h_{2,i,j}^n = H_{i,j}^n \text{ and } S_{i,j} = 0 \\ &\Rightarrow q_{2x,i,j}^{n+1} = q_{2x,i,j}^{n+1*} = q_{2x,i,j}^n \quad q_{2y,i,j}^{n+1} = q_{2y,i,j}^{n+1*} = q_{2y,i,j}^n \text{ and } Q_{i,1}^{n+1} = Q_{1,i}^{n+1*} = Q_{1,i}^n \\ &\Rightarrow q_{x,i,j} := h_{1,i,j}^{n+1} \frac{Q_{1,i}^{n+1}}{A_{1,i}^{n+1}} + q_{2y,i,j}^{n+1} = h_{1,i,j}^n \frac{Q_{1,i}^n}{A_{1,i}^n} + q_{2y,i,j}^n = q_{x,i,j}^n \\ &\text{and } q_{y,i,j}^{n+1} := H_{i,j}^{n+1} \frac{q_{2y,i,j}^{n+1}}{h_{2,i,j}^{n+1}} = H_{i,j}^n \frac{q_{2y,i,j}^n}{h_{2,i,j}^n} = q_{y,i,j}^n. \end{aligned}$$

We have shown that $H_{i,j}^{n+1} = H_{i,j}^n$, $q_{x,i,j}^{n+1} = q_{x,i,j}^n$ and $q_{y,i,j}^{n+1} = q_{y,i,j}^n$, so the method is well-balanced.

□

Theorem 5.4 (Conservation) *If the intermediate solutions is mass conservative, then the vertical coupling solutions is also mass conservative.*

Proof: Let the intermediate solutions be mass conservative, then

$$\sum_i A_{1,i}^{n+1*} = \sum_i A_{1,i}^n \text{ and } \sum_i A_{2,i}^{n+1*} = \sum_i A_{2,i}^n. \quad (119)$$

Hence

$$\begin{aligned} \sum_i (A_{1,i}^{n+1} + A_{2,i}^{n+1}) &:= \sum_i (A_{1,i}^{n+1*} + A_{2,i}^{n+1*}) \quad (\text{see (98)}) \\ &= \sum_i (A_{1,i}^n + A_{2,i}^n) \quad (\text{see (119)}). \end{aligned}$$

□

In the following, we prove that the proposed schemes for the intermediate solutions satisfy the desirable properties. Since the hydrostatic reconstruction method is mass conservative, [2, 1] and the 2D models, (91) do not introduce any source term to the height equation, then the scheme (111) is mass conservative. We state and prove a theorem below to show that this scheme, like the standard hydrostatic reconstruction [1] method, preserves well-balance of lake at rest.

Theorem 5.5 *The upper layer scheme in (111) is well-balanced with respect to lake at rest.*

Proof: Let the flow satisfy the lake at rest condition, then $\eta_{k,L}^n = \eta_{k,R}^n$ and $\vec{q}_{2,i,j}^n = 0$. Hence by (112), we have

$$\begin{aligned} \tilde{h}_{2,k,L}^n &:= \max(\eta_{k,L}^n - \eta_{1,k'}^{n*}, 0) \\ &= \max(\eta_{k,R}^n - \eta_{1,k'}^{n*}, 0) \quad (\text{because } \eta_{k,L}^n = \eta_{k,R}^n) \\ &= \tilde{h}_{2,k,R}^n \quad (\text{by definition}). \end{aligned} \quad (120)$$

Hence

$$\begin{aligned} \tilde{U}_{2,k,R}^n &:= \frac{\tilde{h}_{2,k,R}^n}{h_{2,k,R}^n} U_{2,k,R}^n = (\tilde{h}_{2,k,R}^n, 0, 0)^T \\ &= (\tilde{h}_{2,k,L}^n, 0, 0)^T \quad (\text{see (120)}) \\ &= \tilde{U}_{2,k,L}^n. \end{aligned}$$

Therefore, by the consistency of numerical flux function, we have

$$\phi^{2D}(\tilde{U}_{2,k,L}^n, \tilde{U}_{2,k,R}^n, \vec{n}_k) = \begin{pmatrix} 0 \\ \frac{g}{2} (\tilde{h}_{2,k,L}^n)^2 \vec{n}_k \end{pmatrix}.$$

Hence the scheme, (111) becomes

$$\begin{aligned} U_{2,i,j}^{n+1*} &= U_{2,i,j}^n - \frac{\Delta t}{|T_{ij}|} \sum_{e_k \in \mathcal{E}_{ij}} |e_k| \left[\left(0, \frac{g}{2} (\tilde{h}_{2,k,L}^n)^2 \vec{n}_k \right)^T + \frac{g}{2} \left(0, ([h_{2,i,j}^n]^2 - [\tilde{h}_{2,k,L}^n]^2) \vec{n}_k \right)^T \right] \\ &= U_{2,i,j}^n - \frac{\Delta t}{|T_{ij}|} \sum_{e_k \in \mathcal{E}_{ij}} |e_k| \left[\frac{g}{2} \left(0, (h_{2,i,j}^n)^2 \vec{n}_k \right)^T \right] \\ &= U_{2,i,j}^n - \frac{\Delta t}{|T_{ij}|} \frac{g}{2} (h_{2,i,j}^n)^2 \sum_{e_k \in \mathcal{E}_{ij}} \left[\left(0, \vec{n}_k |e_k| \right)^T \right] = U_{2,i,j}^n. \end{aligned}$$

□

Theorem 5.6 *If the underlying solver for (114) is well-balanced then the lower layer scheme, (117) is also well-balanced.*

Proof: Let scheme for (114) be well-balanced, then $(A_i^{n+1*}, Q_i^{n+1*})^T = (A_i^n, Q_i^n)^T$. Since the 2D solver, (111), is also well-balanced, so $(h_{2,i,j}^{n+1*}, \bar{q}_{2,i,j}^{n+1*})^T = (h_{2,i,j}^n, \bar{q}_{2,i,j}^n)^T$. Therefore, the lower layer scheme, (117) becomes

$$\begin{aligned} \begin{pmatrix} A_{1,i} \\ Q_{1,i} \end{pmatrix}^{n+1*} &:= \begin{pmatrix} A_i \\ Q_i \end{pmatrix}^{n+1*} - \begin{pmatrix} A_{2,i} \\ Q_{2,i} \end{pmatrix}^{n+1*} = \begin{pmatrix} A_i \\ Q_i \end{pmatrix}^n - \begin{pmatrix} A_{2,i} \\ Q_{2,i} \end{pmatrix}^n \\ &= \begin{pmatrix} A_{1,i} \\ Q_{1,i} \end{pmatrix}^n \end{aligned}$$

So, the 1D scheme is well-balanced. \square

Theorem 5.7 *If the underlying solver for (114) is mass conservative, then the lower layer scheme, (117) is also mass-conservative.*

Proof: Let scheme for (114) be mass conservative, then $\sum_i A_i^{n+1*} = \sum_i A_i^n$. Since the 2D solver, (111), is also mass conservative, so $\sum_i A_{2,i}^{n+1*} = \sum_i A_{2,i}^n$. Therefore, the lower layer scheme, (117) gives

$$\begin{aligned} \sum_i A_{1,i}^{n+1*} &:= \sum_i A_i^{n+1*} - \sum_i A_{2,i}^{n+1*} \\ &= \sum_i A_i^n - \sum_i A_{2,i}^n \quad (\text{by conservation of } A_i^{n+1} \text{ and } A_{2,i}^{n+1*}) \\ &= \sum_i (A_i^n - A_{2,i}^n) = \sum_i A_{1,i}^n \quad (\text{by definition}). \end{aligned}$$

So, the 1D scheme is mass conservative. \square

Since we use the 1D solver in [17] which is conservative and well-balanced for lake at rest, and the 2D scheme, (111) is also mass conservative and well-balanced for lake at rest, therefore by theorems 5.4 and 5.3 the vertical coupling scheme, (106), (108), (109) is mass conservative and well-balanced for lake at rest.

This completes the theoretical aspect of the VCM. In the next chapter, we present some numerical experiments to access the its performance.

6 Numerical Results

We now present some numerical results to access the performance of the method. All the algorithms described in this paper are implemented in an in-house C++ code. The experiments are run on the Cluster of Workstations (COW) of the Center for Scientific Computing (CSC), University of Warwick. The CSC's COW is a heterogeneous cluster with approximately 600 cores for code development and computations.

As stated before, the VCM is a unifying method depending on the choice of the elevation function, $z_b^w(x)$. Here, we give some examples to explain this. Recall that if the channel is full, then $z_b^w(x)$ is the interface boundary between the lower and upper layers. Therefore, a change in the choice of $z_b^w(x)$ would change the position of the interface and ultimately change the type of method. For instance,

- If

$$z_b^w(x) = Z_b(x) \text{ for all } x, \quad (121)$$

where $Z_b(x)$ is the bottom of the channel, then the vertical coupling method becomes a full 2D simulation because the lower layer no longer exists and upper layer model reduces to the full 2D shallow water equations.

- If

$$z_b^w(x) = \infty \text{ for all } x, \quad (122)$$

then the vertical coupling method reduces to the Horizontal Coupling Method (HCM) [20, 21]. This is true because the upper layer vanishes and the solution of the lower layer model, as approximated in section 4.5.2, reduces to that of the channel model with coupling term in HCM.

- Suppose it is known a priori that the channel never floods in some region, $\Omega_{nF} \in \mathbb{R}$ and there are other region, $\Omega_F \in \mathbb{R}$ in which the channel is most likely to flood, say where the channel flows into a floodplain, then we can define

$$z_b^w(x) = \begin{cases} 0, & \text{if } x \in \Omega_F, \\ \infty, & \text{if } x \in \Omega_{nF}, \end{cases} \quad (123)$$

and we ensure that $z_b^w(x)$ varies smoothly between Ω_F and Ω_{nF} . In this case, the vertical coupling method, is automatically a flow direction or frontal coupling method. Frontal or flow direction coupling method is the approach used to couple a 1D and 2D models when the 2D domain is in the direction of the 1D flow.

- If we define $z_b^w(x)$ to be the minimum channel bank elevation, as we did in this paper, then the method is a purely vertical coupling method, different from any existing method.

In this paper, we do not consider all the cases but only focus on the last case in which we take $z_b^w(x)$ as the minimum bank elevation. Before we continue, let us make the following remark.

Remark 6.1 *We observed that if the choice of $z_b^w(x)$ has very large gradients, then it leads to numerical difficulties. Hence, we propose to smooth-en $z_b^w(x)$ whenever it has large gradients. Therefore, for each test case below, given $z_b^w(x)$, we also state the corresponding smooth version (when necessary). But the point to note is that in reality, $z_b^w(x)$ would not have vary large gradients to warrant smoothing.*

6.1 Test Case 1 : Dam-Break Flow into a Flat Floodplain

The first test case is the problem considered in [17]. This problem consists of a dam break flow in a 19.3 meter long, 0.5 meter constant width flat channel which ends into a flat floodplain, see figure 11. The National Laboratory of Civil Engineering in the IST in Portugal designed and measured this test case [25, 17]. A reservoir is located from the left end of the channel to 6.10 metres away (position of dam in figure 11). The initial condition is

$$H(x, y, 0) = \begin{cases} 0.504, & \text{at the reservoir, that is } 0 \leq x \leq 6.10 \text{ and } 1.8 \leq y \leq 2.3, \\ 0.003, & \text{elsewhere,} \end{cases}$$

$$u(x, y, 0) = v(x, y, 0) = 0 \quad \text{everywhere.}$$

The manning coefficient for both channel and floodplain is $0.009\text{s/m}^{1/3}$ and the boundaries are all closed walls except the right side as indicated in figure 11. The labels P_1, P_2, \dots, P_6 are probe points in the flow domain. More about this test case can be found in [17, 25].

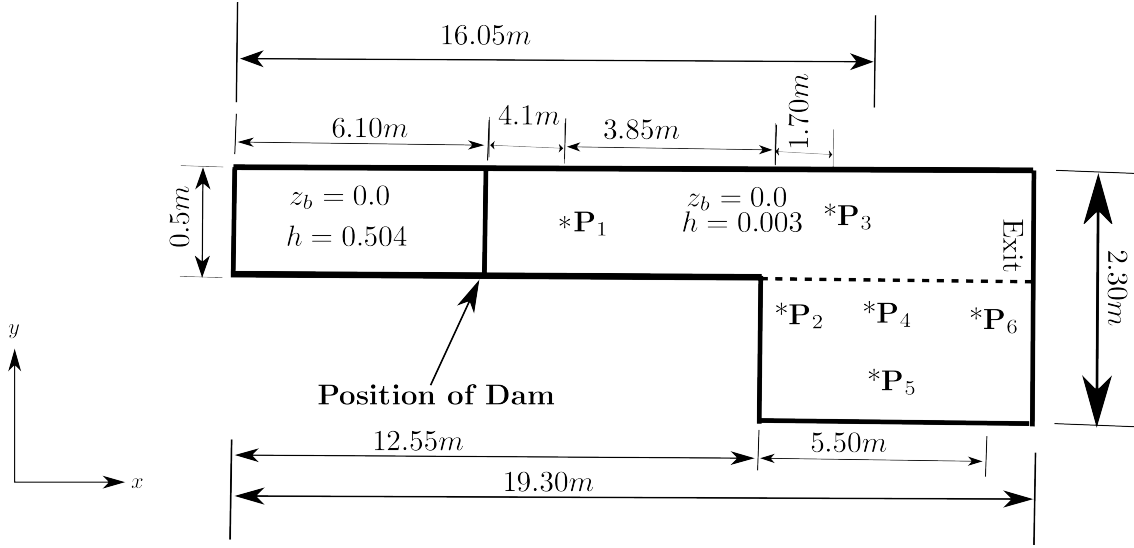


Figure 11: Top view of Channel and Floodplain for river-flooding problem

For this test case, the channel wall elevation, $z_b^w(x)$ is given as

$$z_b^w(x) = \begin{cases} 2.5, & \text{if } x \leq 12.50, \\ 0.0, & \text{elsewhere.} \end{cases} \quad (124)$$

We use the following smoother version of $z_b^w(x)$ for the VCM.

$$z_b^w(x) = \begin{cases} \tanh((x - 10.0)) + 1.0, & \text{if } x < 14.0, \\ 0.0, & \text{if } x \geq 14.0. \end{cases} \quad (125)$$

6.1.1 Result of test 1: Here, a full 2D simulation was run with a grid of 193×115 cells (193×90 in the floodplain and 193×25 in the channel), the HCM was run on a grid made of 193×90 cells in the floodplain and 193×2 cells in the channel, the FBM with a grid of 193×90 in the floodplain and 193×1 in the channel, while the VCM is run with a grid of 193×90 cells in the floodplain and 8 cells in lateral direction in the channel, making a total of 193×198 non-uniform grid cells, (see table 1). Each simulation was run for ten seconds with a CFL number of 0.95.

Figure 12 displays the free surface elevation for the various methods after the last time step. It is very obvious that the vertical coupling method approximates the full 2D simulation result better than the horizontal coupling method. The accuracy of the vertical coupling method is further illustrated in figure 13 which displays the free surface elevation, over time, at the six probe points. It can be seen that the VCM captures the full 2D results very well than the horizontal coupling method, at all the probe points. Again, from figure 12, one can see that the VCM recovers 2D flow structure within the channel unlike the HCM and FBM. Again, this 2D flow structure is only within the flooded region, while non-flooded regions remain with 1D solutions. In terms of efficiency, table 1 shows that for this test case, the vertical coupling method has about 48.39% gain in computational time over the full 2D simulation.

6.2 Test case 2 : Channel Flow into Elevated 2D Floodplain

This test case involves the same channel in the previous test case but connected to an elevated floodplain located in the region $10.5 \leq x \leq 16.0$ (see figure 14). The channel bed is flat and the

	Grid	No. of time steps	Processor time (in seconds)
Full 2D	193 × 115	3,669	3,110.31
VCM	193 × 98	2,615	1,605.31
HCM	193 × 92	2,616	1,420.40
FBM	193 × 91	2,592	1,311.26

Table 1: Grid cells, simulation times and number of time steps : Test 1

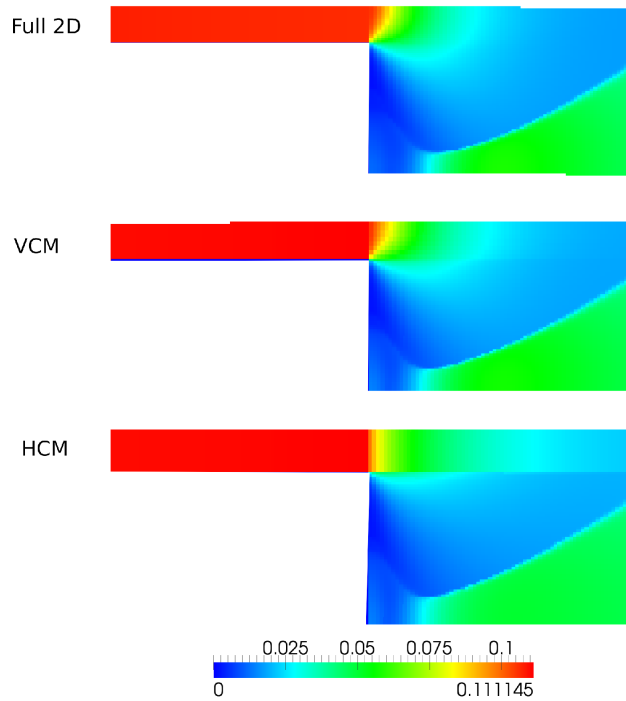


Figure 12: Comparison of free surface elevation for the different methods: Test 1

floodplain bed is 0.5 meters high. The initial condition is the following.

$$H(x, y, 0) = \begin{cases} 1.5, & \text{if } x \leq 8.5, \quad y \geq 1.8, \\ 0.7, & \text{if } x > 8.5, \quad y \geq 1.8, \\ 0.2, & \text{if } 10.5 \leq x \leq 16.0, \quad 0 \leq y \leq 1.8, \\ 0.0, & \text{else.} \end{cases} \quad (126)$$

$$u(x, y, 0) = v(x, y, 0) = 0. \quad (127)$$

The manning coefficient for both channel and floodplain is taken as $0.009s/m^{1/3}$ the boundaries are only open at the sides indicated "exit" in figure 14, others are closed. Nine probe points are considered, see figure 14.

To apply the vertical coupling method to this problem, we first realize that from the bottom

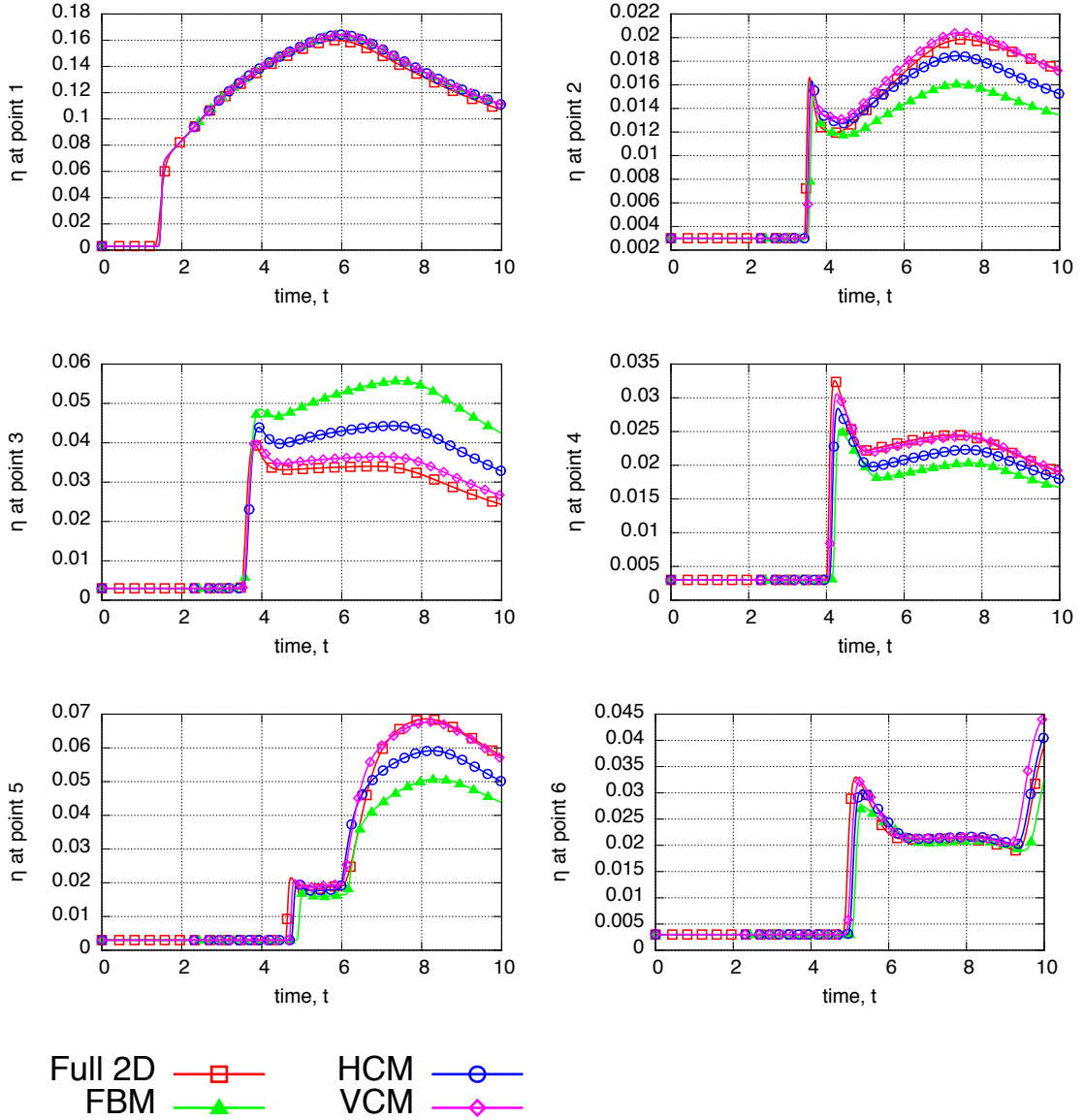


Figure 13: Comparison of free surface elevation at probe points : Test 1

topography of the channel and bed given above, the channel wall elevation, $z_b^w(x)$ is given as

$$z_b^w(x) = \begin{cases} 0.5, & \text{if } 10.5 \leq x \leq 16.0, \\ 3.0, & \text{elsewhere.} \end{cases} \quad (128)$$

The smoother version used for the VCM is the following

$$z_b^w(x) = \begin{cases} \tanh(0.5(x - 4.5)) + 1.5, & \text{if } x < 10.0, \\ 0.5, & \text{if } 10.0 \leq x \leq 16.5, \\ \tanh(x - 19.2) + 1.5, & \text{elsewhere.} \end{cases} \quad (129)$$

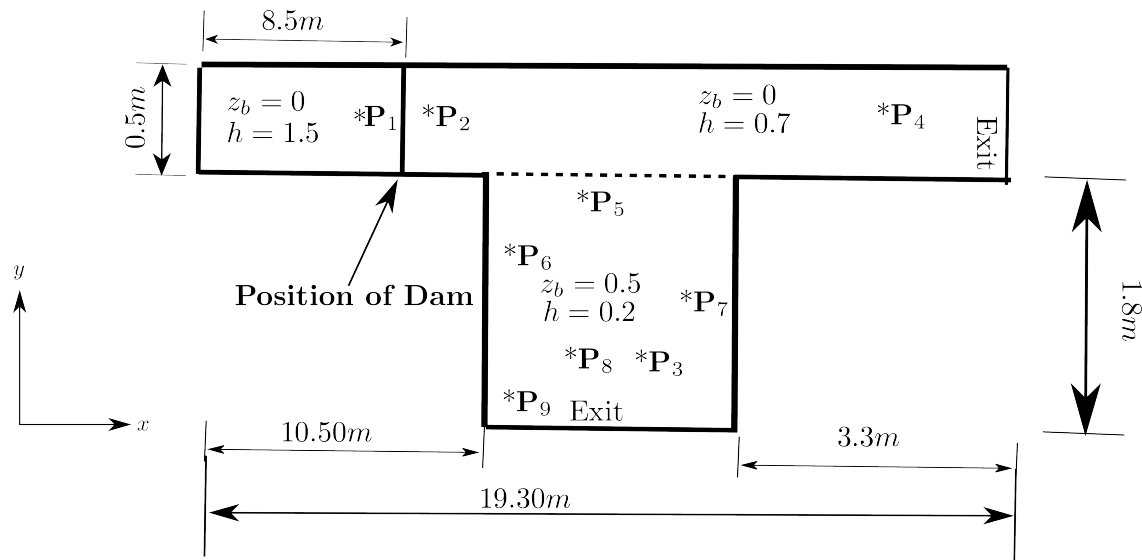


Figure 14: Top view of Channel and Floodplain for Test 2

6.2.1 Result of test 2: The vertical coupling method and the other three methods simulated this problem with their respective grid for the previous problem. This is shown under the grid column in table 2. The simulation was run for ten seconds.

Figures 15 and 16 show the free surface elevation and velocity magnitude for each method. It can be seen that the vertical coupling method provides a better approximation of the full 2D results than the horizontal coupling method which in turn, is more accurate than the FBM. As further validation of this claim, the free surface elevation, the x-component and y-component velocity are plotted for selected probe points in figures 17, 18 and 19 respectively. It can be seen that the vertical coupling method is more accurate than the other methods for all three flow quantities, at the reported points and almost throughout the duration of simulation. And the horizontal coupling method is more accurate than the FBM at the points for all flow quantities and almost all the time. Again, the vertical coupling method really captures the flow structure of the full 2D simulation.

	Grid	No. of time steps	Processor time (in seconds)
Full 2D	193×115	4,963	4,100.47
VCM	193×98	3,278	2,811.00
HCM	193×92	3,235	1,710.36
FBM	193×91	3,178	1,555.08

Table 2: Grid cells, simulation times and number of time steps : Test 2

For efficiency, we see from column under processing time in table 2 that the FBM is very efficient but not very accurate, the vertical coupling method is also efficient compared to the full 2D but not as much as the other two methods, while the horizontal coupling method is both very efficient and also has good accuracy. For this problem, due to the very high accuracy of the vertical coupling method, it is sensible to conclude that it is the best amongst the three coupling methods. Moreover, for a simulation of a very large network of rivers where the 2D region might be very small compared to the entire computational domain, the efficiency of one coupling method over the other might not be very significant, so accuracy becomes the deciding factor. In this regard, the vertical coupling method is the best method of the three considered here.

Finally, figures 12 and 16 show that the VCM, unlike the other methods, recovers the 2D flow structure within the channel at the flooding regions. Again, the VCM continues to compute 1D solutions at no flooded regions; this demonstrates the self-adaptive nature of the method.

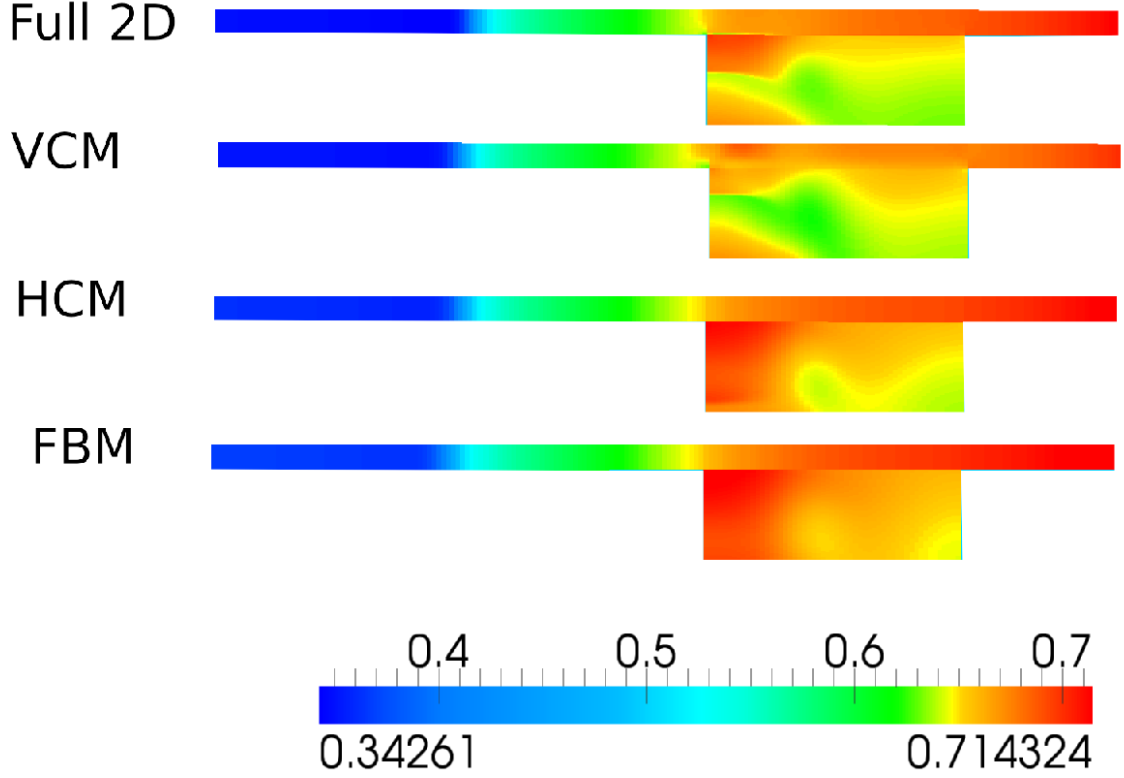


Figure 15: Comparison of free surface elevation for the different methods: Test 2

6.3 Test case 3 : Flooding of an initially dry floodplain

The final test case involves the overflowing of a channel onto an initially dry floodplain. Both the channel and the floodplain are located in the 2D domain, $[0, 20] \times [0, 4]$. The channel occupies the region, $[0, 20] \times [y_c, 4]$ with flat bottom, $Z_b(x) = 0$, while the floodplain occupies the rest of the domain, $[0, 20] \times [0, y_c]$, where $y_c = 3$. The bottom topography of the entire domain is the following

$$z_b(x, y) = \begin{cases} Z_b(x) = 0, & \text{if } y \geq y_c, \\ 0.2 + \frac{z_b^w(x) - 0.2}{y_c} y, & \text{otherwise.} \end{cases} \quad (130)$$

where $z_b^w(x)$ is the channel wall elevation function defined as

$$z_b^w(x) = \begin{cases} -0.06 \tanh(3(x - 9)) + 0.14, & \text{if } x \leq 10.5, \\ 0.06 \tanh(3(x - 15.5)) + 0.14, & \text{otherwise.} \end{cases} \quad (131)$$

For this problem, we take $z_b^w(x)$ the way it is. The bed and channel wall elevations are depicted in figure 20.

The initial condition consists of stationary water of depth, 0.08 meters in the channel and dry floodplain. The boundary conditions are time-dependent water depth at the left boundary of the

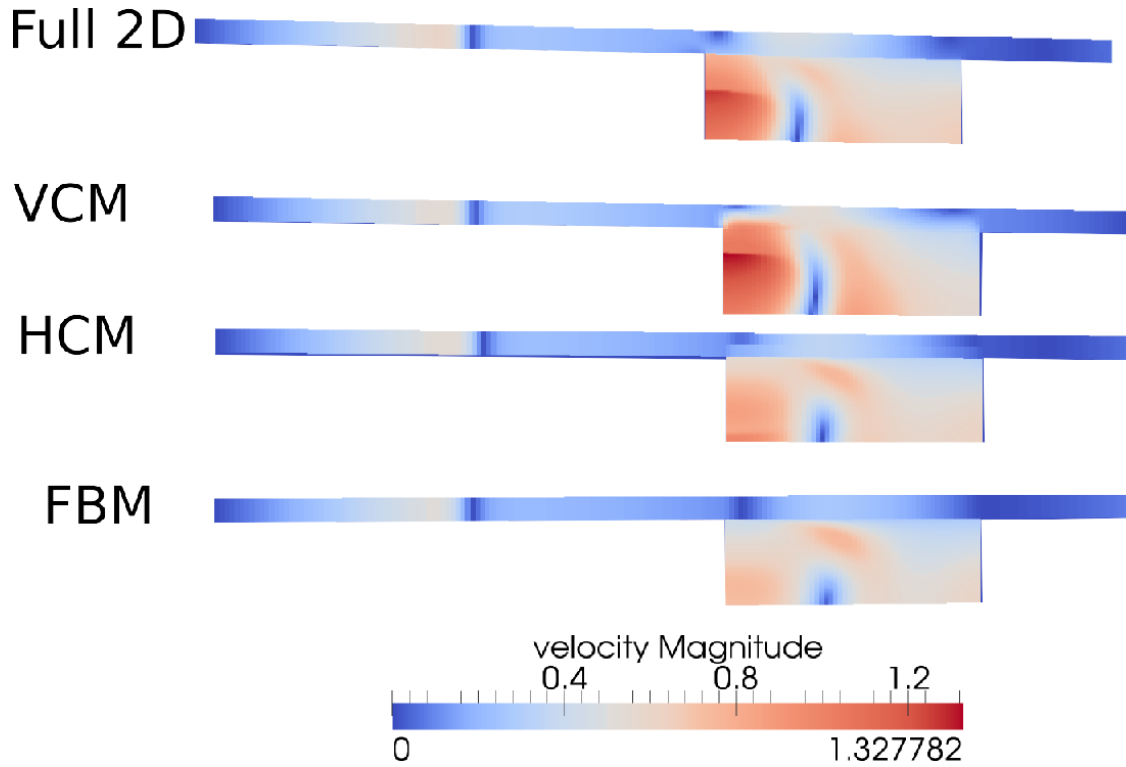


Figure 16: Comparison of velocity magnitude for the different methods: Test 2

channel and zero velocity at the right channel boundary, namely

$$H(0, y, t) = \begin{cases} h_b(t), & \text{if } t \leq 4a, \\ h_b(4a), & \text{if } t > 4a, \end{cases} \quad (132)$$

for $y \geq y_c$,

$$u(20, y, t) = 0.0, \text{ for all } t \geq 0, y \geq y_c, \quad (133)$$

where

$$h_b(t) = \eta_0 + r + r \sin\left(\frac{(t-a)\pi}{2a}\right). \quad (134)$$

where $a = 10$ and $r = 0.025$. $\eta_0 = 0.08$ is a constant initial free-surface elevation inside the channel. The remaining boundaries are closed.

The manning coefficients are the same as used in the previous cases. The following probe points are chosen, $P_1(2.5, 3.5)$, $P_2(4.0, 3.8)$, $P_3(7.0, 3.3)$, $P_4(10.0, 3.4)$, $P_5(11, 3.5)$, $P_6(12, 3.3)$, $P_7(14, 3.4)$, $P_8(16, 3.5)$, $P_9(17.3, 3.5)$, $P_{10}(19, 3.5)$, $P_{11}(12, 2.8)$, $P_{12}(13, 2.8)$, $P_{13}(12, 2.5)$, $P_{14}(12, 2.0)$ and $P_{15}(13.0, 1.0)$.

6.3.1 Discussion of Results of test case 3: Table 3 shows the domain discretization for both the channel and floodplain for each method being discussed. As before, all methods use the same grid for the floodplain but different grids for the channel. This problem was simulated for $t = 100$ seconds. We report, in figures 21 - 24, the results of the simulation after 40 seconds and in figures 25 and 26, we report the results at selected probe points throughout the duration of the simulation.

As can be seen from the pictures, all the coupling methods provide very good approximation of full 2D simulation results for both the free surface elevation (figure 21), the velocity components

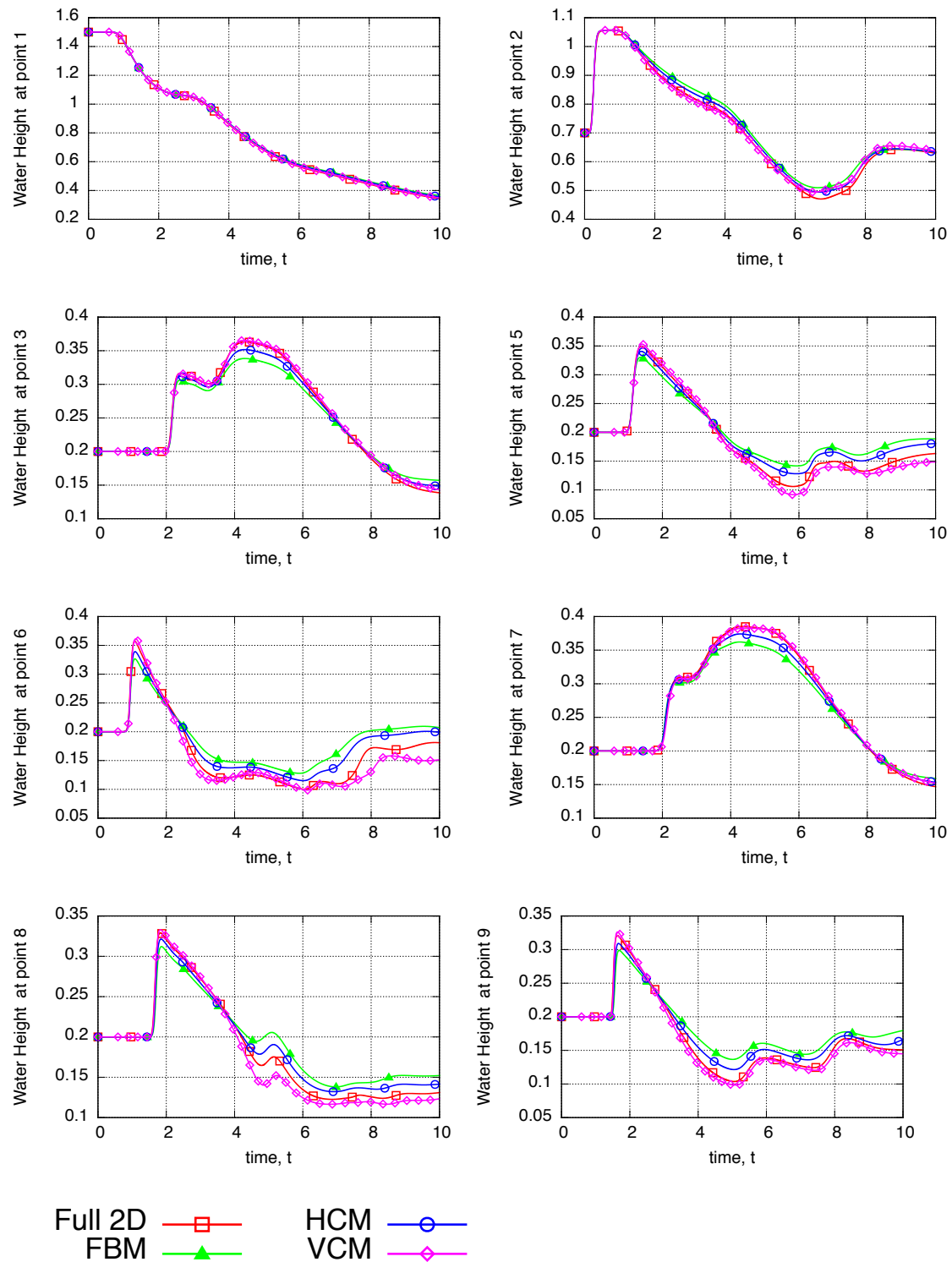


Figure 17: Comparison of water height at probe points : Test 2

(figures 22 and 23) and the velocity magnitude (figure 24) for this test case. However, as one can see from these pictures, the VCM provides more smooth variation of flow variables between

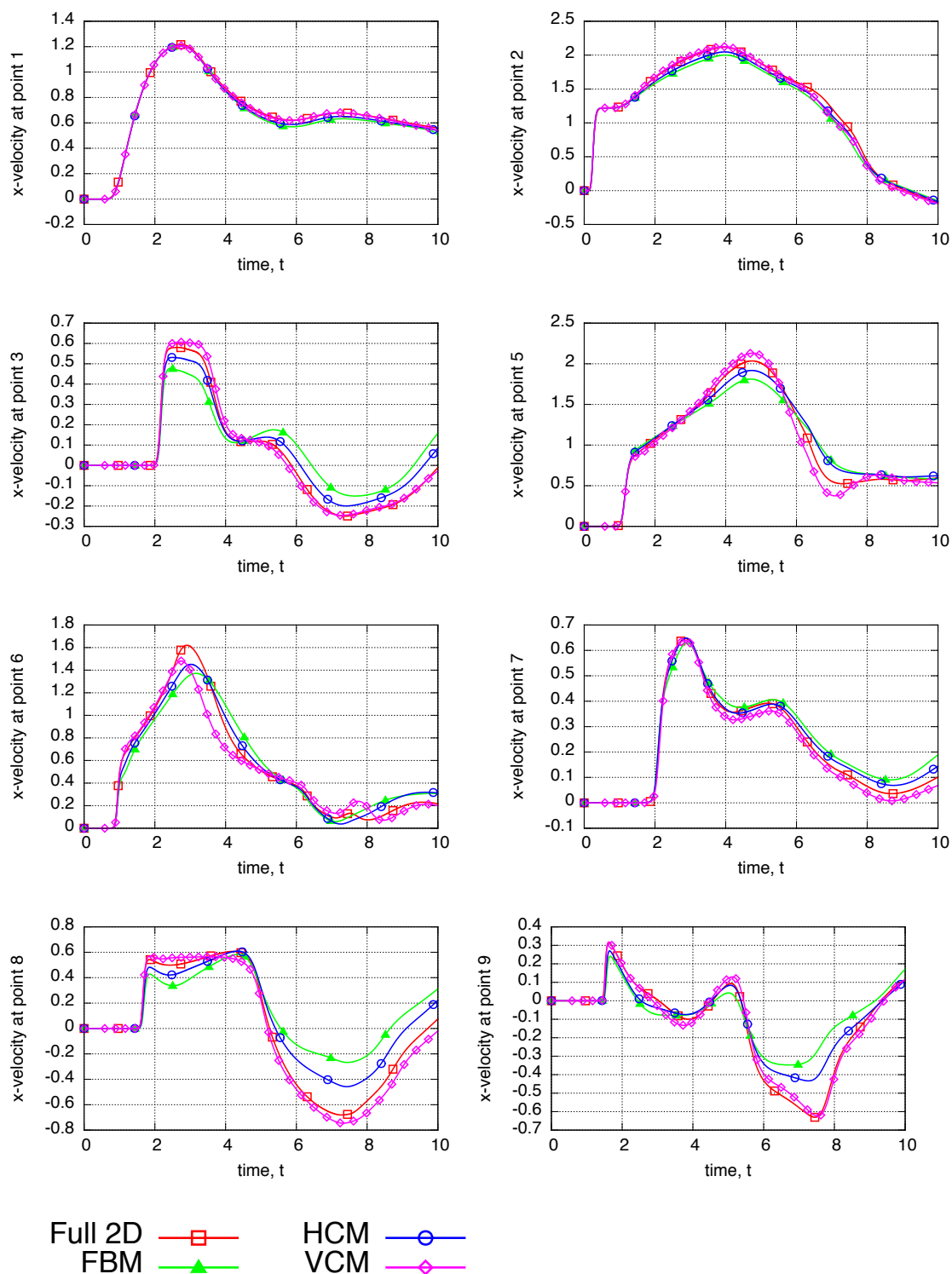


Figure 18: Comparison of x-velocity at probe points : Test 2

the channel and the floodplain. That is, all flow variables vary smoothly from the channel to the floodplain. This is not so for the other coupling methods. Again, the lateral variation of

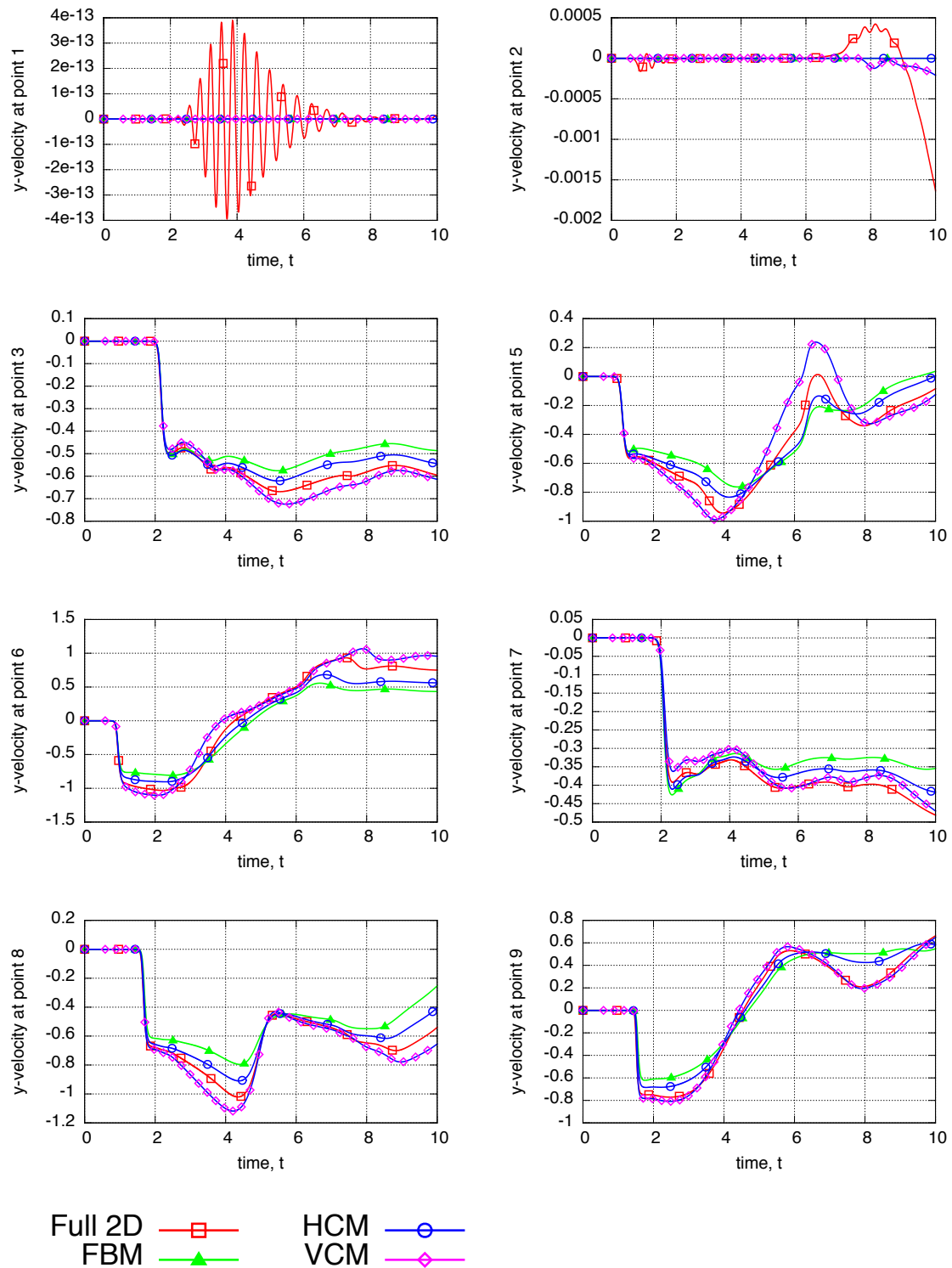


Figure 19: Comparison of y-velocity at probe points : Test 2

flow quantities within the channel during flooding, is properly captured by the vertical coupling method than the other methods. This demonstrates the ability of the VCM to recover 2D flow

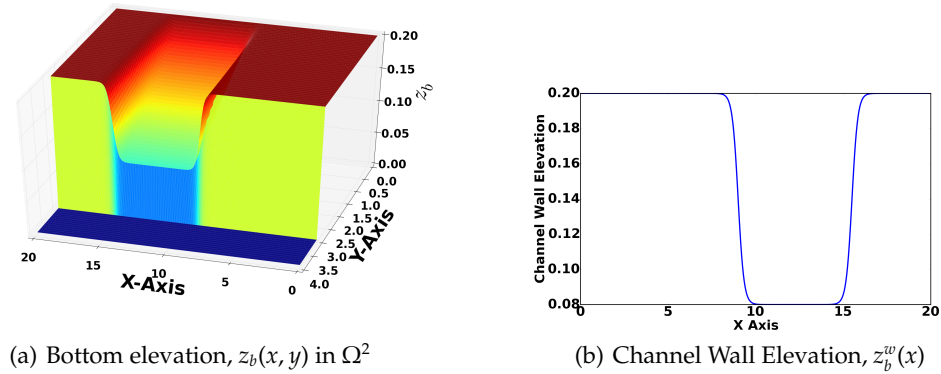


Figure 20: The 2D bed elevation and channel wall elevation for test 3

structure unlike most existing methods.

And in terms of accuracy of y-velocity component, the VCM and HCM provide better approximations than the FBM as can be seen in figure 23.

	Channel Grid	Floodplain Grid
Full 2D	600 × 30	600 × 90
VCM	600 × 10	600 × 90
HCM	600 × 2	600 × 90
FBM	600 × 1	600 × 90

Table 3: Grid cells, simulation times and number of time steps : Test 3

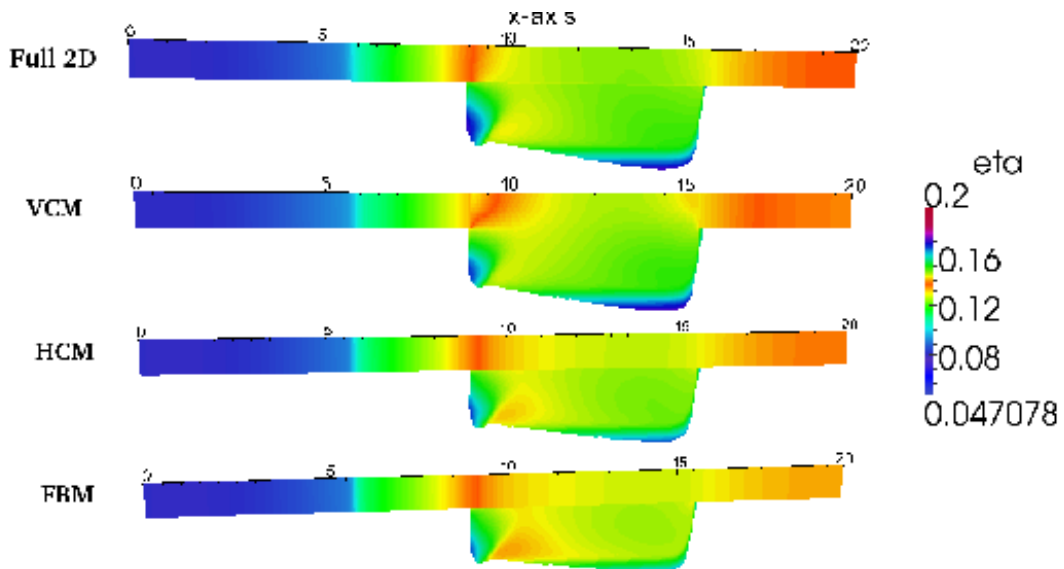


Figure 21: Visualisation of free surface elevation after t=40s for test 3

To further understand the results of the simulations, the flow quantities over time at the probe points, $P_1 - P_{15}$ have been examined. Here we report the results at the probe points P_1, P_4, P_5, P_6

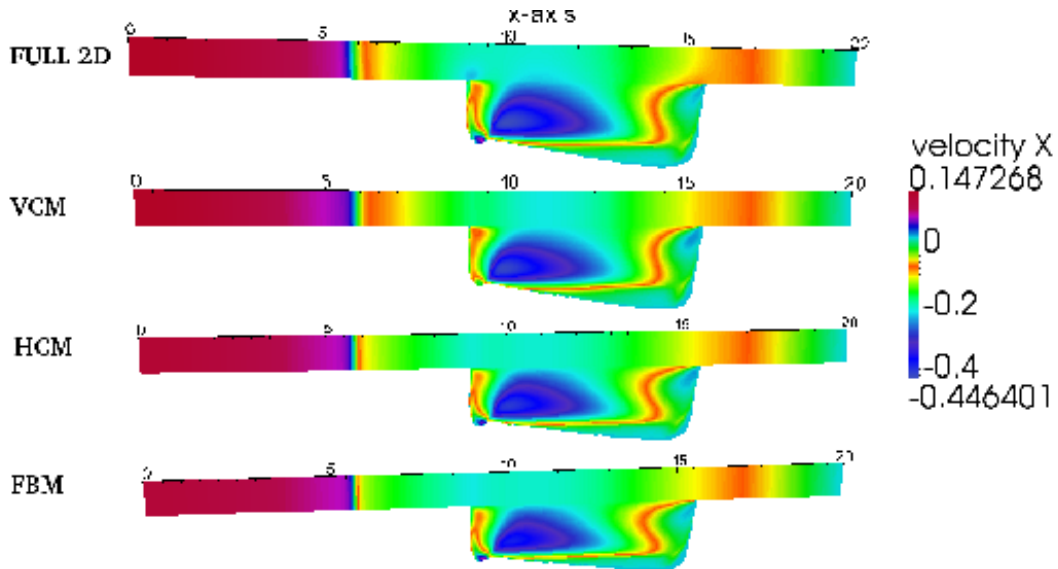


Figure 22: Visualisation of x -velocity after $t=40s$ for test 3

which are in the channel and the points, P_{11}, P_{12}, P_{13} and P_{14} in the floodplain. Figures 25 and 26 show the results for the selected points in the channel and floodplain respectively. In each figure, the left column displays the water depth, the second (middle) column shows the x -component of velocity, while the third (right) column shows the y -component of velocity.

From figure 25, we can see that all the coupling methods provide very good approximation of the results of the full 2D simulations, especially for the water depth and x -component of velocity. The y -velocity is truly small within the channel and only the VCM and HCM are able to compute its small variations in the channel. This is also true for the probe points not reported here.

From figure 26, we also see that for the points in the floodplain, the coupling methods computed very good approximations of results of the full 2D simulation with the HCM and VCM computing more accurate results especially for the y -velocity. This figure also verify the no-numerical flooding property of the methods. That is, the floodplain initially remained dry until the time when water height rose above the channel banks. This is the reason why, for all points in the floodplain, the water depth and velocity remained at zero for the first several seconds of the simulation. Another thing to note is that due to the time-dependent boundary condition provided for this problem, water flew onto the floodplain and after sometime the level of water in the channel decreased, so water in the floodplain drained back into the channel leaving the floodplain dry again. The coupling methods truly capture this phenomenon as one can see in figure 26 where the water depth and velocity return to zero towards the end of the simulation and remain at zero throughout the remaining times of the simulation. This is true for all the points in the floodplain, even those not reported here.

The well-balance property of the methods are also exhibited here. The points in the channel are numbered according to their distance from the left channel boundary. So, P_{10} is further than P_8 which is further than P_7 , etc. The boundary condition makes water enter into the channel (which is initially at rest) from this left boundary. Therefore, water wave would get to P_1 before P_3 etc. This is also reproduced by the results. From figure 26, one can see that the arrival times increase with the distances of the points and that all flow quantities remain at their initial state until the time when the wave arrives. This is true for all the points in the channel and even in the floodplain.

In conclusion, while all the three coupling methods computed results with most of the desirable properties, only the VCM is able to compute 2D flow structure within the channel during flooding.

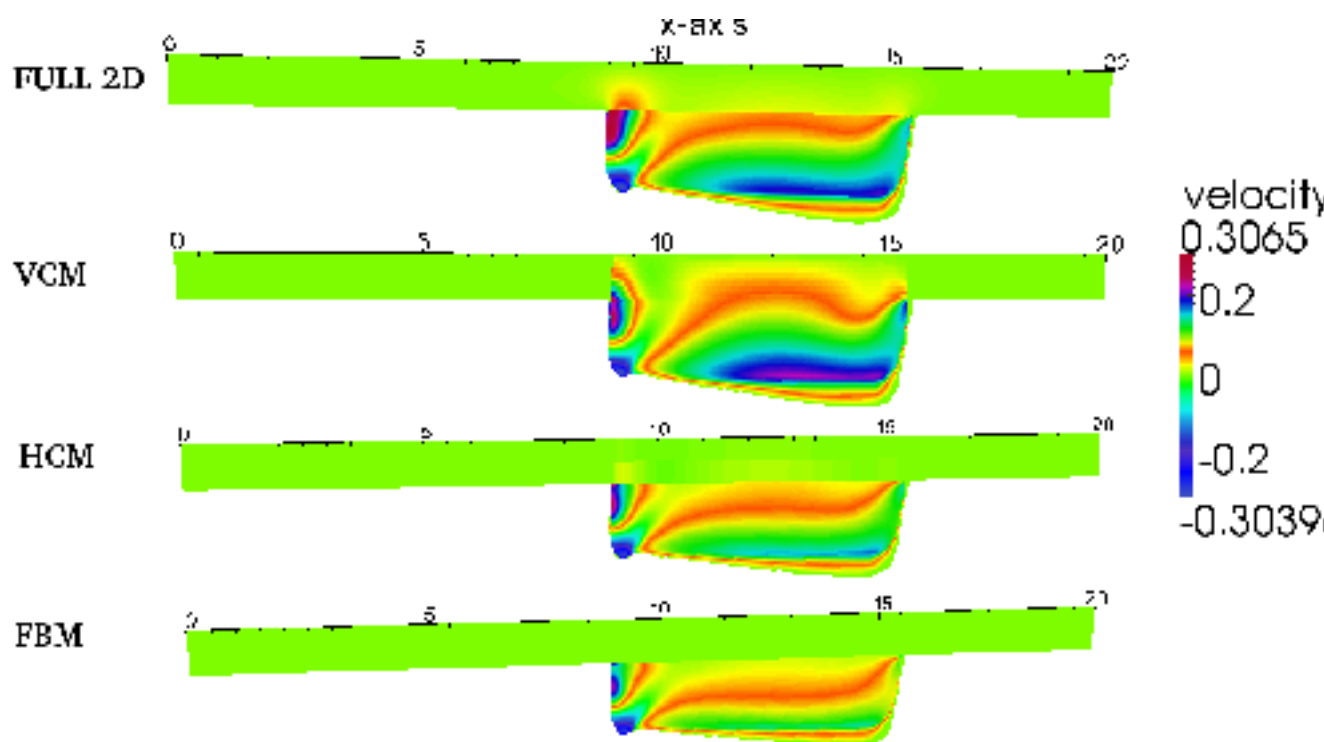


Figure 23: Visualisation of y-velocity after $t=40$ s for test 3

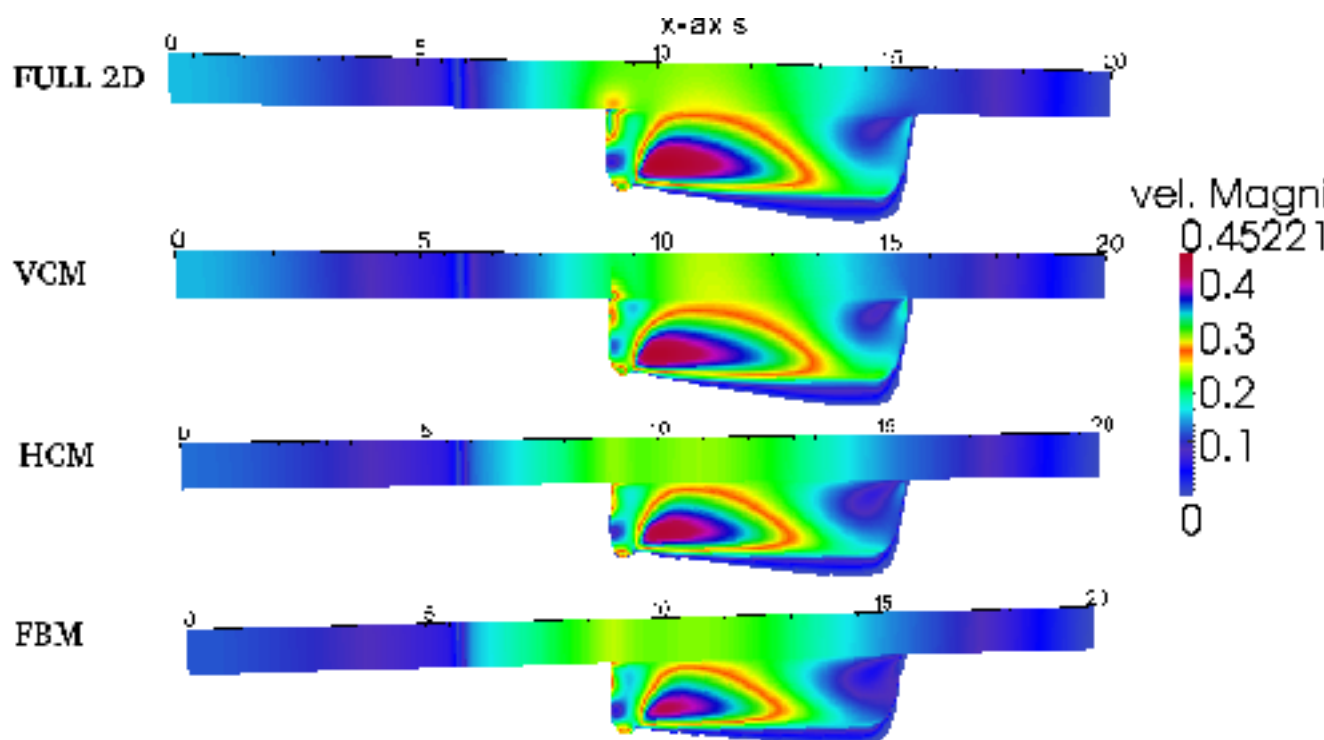


Figure 24: Visualisation of velocity magnitude after $t=40$ s for test 3

This property sets the VCM apart from other coupling methods.

7 Conclusion

The problem of coupling the 2D and 1D shallow water equations have been investigated in this paper. We focused on the need to efficiently recover 2D channel flow structure during flood while maintaining good accuracy. To this end, the vertical coupling method is proposed for the first time. We show that the method truly recovers the 2D flow structure, is a unifying method, mass conservative, well-balanced and preserves the no-numerical flooding property. In addition, the numerical results show that the VCM, in most cases, outperforms the existing methods compared with it in this paper.

Acknowledgement

We are grateful to the Petroleum Technology Development Fund (PTDF), Nigeria for funding this study and to the Centre for Scientific Computing, University of Warwick for providing the computing resources.

References

- [1] E. Audusse, F. Bouchut, M. Bristeau, R. Klein, and B. Perthame. A fast and stable well-balanced scheme with hydrostatic reconstruction for shallow water flows. *SIAM Journal Scientific Computing*, 25:2050–2065, 2004.
- [2] E. Audusse and M. Bristeau. A well-balanced positivity preserving second-order scheme for shallow water flows on unstructured meshes. *Journal of Computational Physics*, 206(1):311–333, 2005.
- [3] E. Audusse, M. Bristeau, B. Perthame, and J. Sainte-Marie. A multilayer saint-venant system with mass exchanges for shallow water flows. derivation and numerical validation. *ESAIM: Mathematical Modelling and Numerical Analysis*, 45(01):169–200, 2011.
- [4] E. Bladé, M. Gómez, and J. Dolz. Quasi-two dimensional modelling of flood routing in rivers and flood plains by means of storage cells. In *Modelling of Flood Propagation Over Initially Dry Areas*, pages 156–170. ASCE, 1994.
- [5] E. Bladé, M. Gómez-Valentín, J. Dolz, J. Aragón-Hernández, G. Corestein, and M. Sánchez-Juny. Integration of 1d and 2d finite volume schemes for computations of water flow in natural channels. *Advances in Water Resources*, 42:17–29, 2012.
- [6] F. Bouchut. *Nonlinear stability of finite Volume Methods for hyperbolic conservation laws: And Well-Balanced schemes for sources*. Springer Science & Business Media, 2004.
- [7] F. Bouchut. *Efficient Numerical Finite Volume Schemes for Shallow Water Models*. Elsevier, 2007.
- [8] Y. Chen, Z. Wang, Z. Liu, and D. Zhu. 1d-2d coupled numerical model for shallow-water flows. *Journal of Hydraulic Engineering*, 138:122–132, 2012.
- [9] J. A. Cunge, F. M. Holly, and A. Verwey. *Practical aspects of computational river hydraulics*. Pitman publishing, 1980.
- [10] E. D. Fernandez-Nieto, J. Marin, and J. Monnier. Coupling superposed 1d and 2d shallow-water models: Source terms in finite volume schemes. *Computers & Fluids*, 39(6):1070–1082, 2010.
- [11] R. Ghostine, I. Hoteit, J. Vazquez, A. Terfous, A. Ghenaïm, and R. Mose. Comparison between a coupled 1d-2d model and a fully 2d model for supercritical flow simulation in crossroads. *Journal of Hydraulic Research*, 53(2):274–281, 2015.

- [12] N. Goutal, M. Parisot, and F. Zaoui. A 2d reconstruction for the transverse coupling of shallow water models. *International Journal for Numerical Methods in Fluids*, 75(11):775–799, 2014.
- [13] A. Harten, P. D. Lax, and B. Van Leer. On upstream differencing and godunov-type schemes for hyperbolic conservation laws. *SIAM review*, 25(1):35–61, 1983.
- [14] I. MacDonald. *Analysis and computation of steady open channel flow*. PhD thesis, University of Reading Reading, UK, 1996.
- [15] J. Marin and J. Monnier. Superposition of local zoom models and simultaneous calibration for 1d-2d shallow water flows. *Mathematics and Computers in Simulation*, 80(3):547–560, 2009.
- [16] M. Morales-Hernández. *Efficient Explicit Finite Volume Schemes for the shallow water equations with solute transport*. PhD thesis, Universidad Zaragoza, 2014.
- [17] M. Morales-Hernández, P. García-Navarro, J. Burguete, and P. Brufau. A conservative strategy to couple 1d and 2d models for shallow water flow simulation. *Computers & Fluids*, 81:26–44, 2013.
- [18] M. Morales-Hernández, P. García-Navarro, and J. Murillo. A large time step 1d upwind explicit scheme ($cfl > 1$): Application to shallow water equations. *Journal of Computational Physics*, 231(19):6532–6557, 2012.
- [19] M. Morales-Hernández, G. Petaccia, P. Brufau, and P. García-Navarro. Conservative 1d–2d coupled numerical strategies applied to river flooding: The tiber (rome). *Applied Mathematical Modelling*, 40(3):2087–2105, 2016.
- [20] C. Nwaigwe. *Coupling Methods for 2D/1D Shallow Water Flow Models for Flood Simulations*. PhD thesis, University of Warwick, United Kingdom, 2016.
- [21] C. Nwaigwe and A. S. Dedner. Derivation and implementation of the horizontal coupling method for 2d/1d shallow water flow models. *In print*, 2016.
- [22] S. D. Seyoun, Z. Vojinovic, R. K. Price, and S. Weesakul. Coupled 1d and noninertia 2d flood inundation model for simulation of urban flooding. *Journal of Hydraulic Engineering*, 138:23–34, 2012.
- [23] E. F. Toro. *Riemann solvers and numerical methods for fluid dynamics: a practical introduction*. Springer Science & Business Media, 1999.
- [24] E. F. Toro. *Shock Capturing Methods For Free-surface Flows*. Wiley, 2001.
- [25] T. Viseu, A. Franco, and A. B. de Almeida. Numerical and computational results of the 2-d biplan model. In *4th Meeting of the Working Group on Dam-Break Modelling (1st CADAM Meeting)*, 1999.

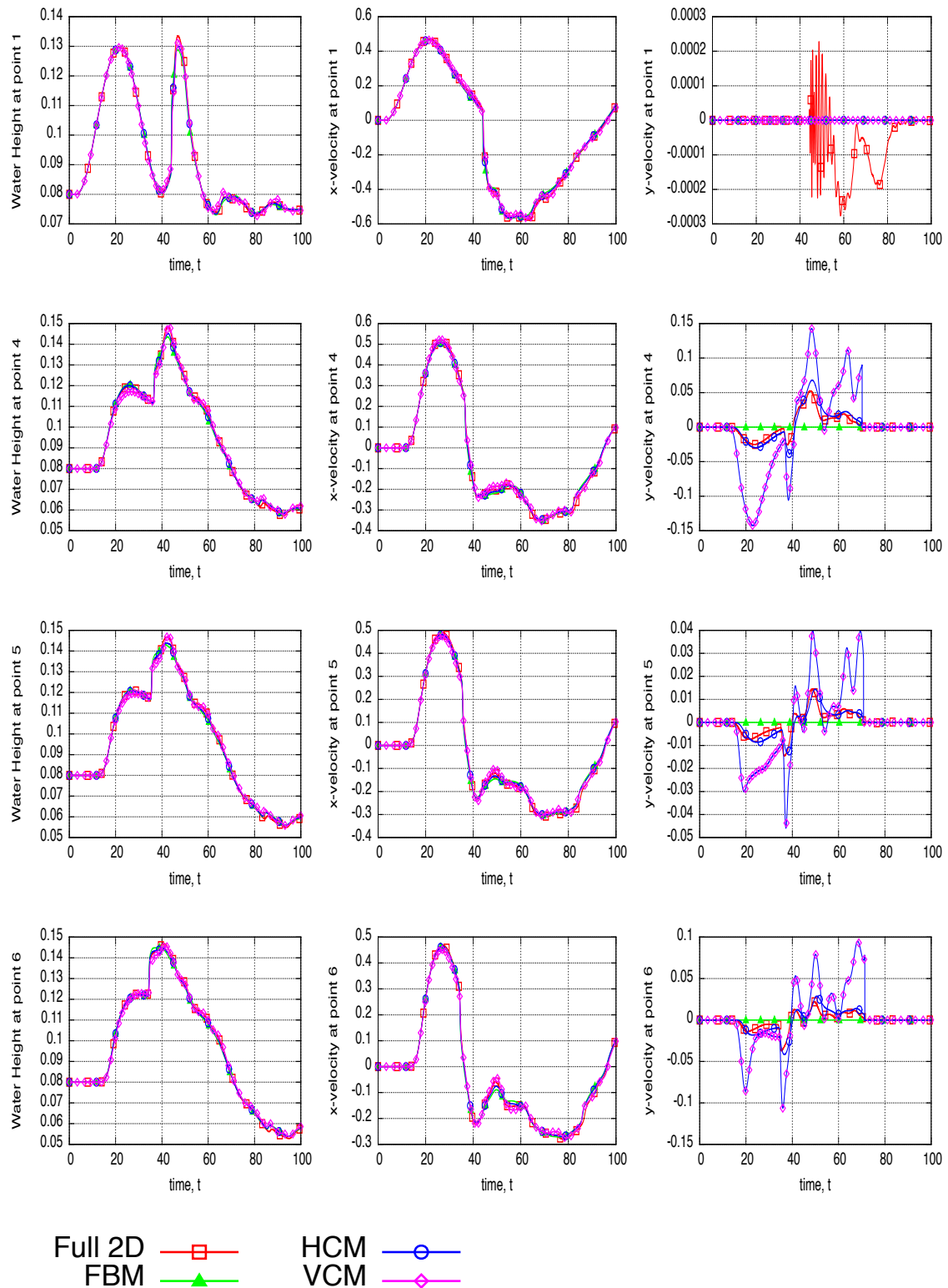


Figure 25: Time variation of water depth H (left column), x -velocity component (middle column) and y -velocity component (right column) at the indicated probe points within the channel for test case 3. Each row corresponds to one probe point.

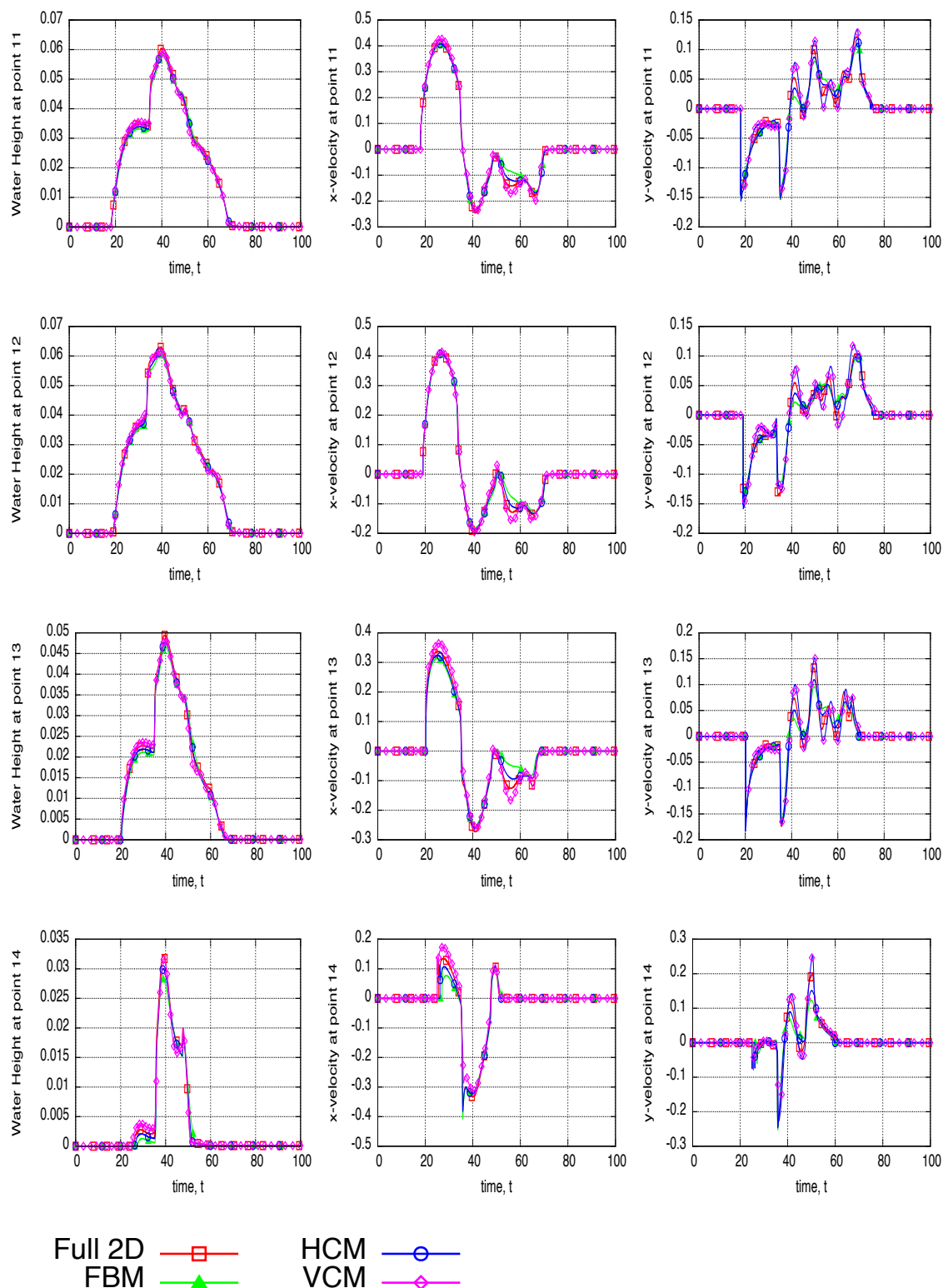


Figure 26: Time variation of water depth H (left column), x -velocity component (middle column) and y -velocity component (right column) at the indicated probe points in the floodplain for test case 3. Each row corresponds to one probe point.